The Pennsylvania State University

The Graduate School

Department of Electrical Engineering

APPLICATIONS OF AN ACOUSTO-OPTIC TUNABLE FILTER IN REMOTE SENSING

A Thesis in

Electrical Engineering

by

Anilkumar V. Nanduri

Submitted in Partial Fulfillment
of the Requirements
for the Degree of

Master of Science

December 1997

The Pennsylvania State University

The Graduate School

Department of Electrical Engineering

APPLICATIONS OF AN ACOUSTO-OPTIC TUNABLE FILTER IN REMOTE SENSING

A Thesis in

Electrical Engineering

by

Anilkumar V. Nanduri

Submitted in Partial Fulfillment
of the Requirements
for the Degree of

Master of Science

December 1997

We approve the thesis of Anilkumar V. Nanduri

Date of Signature

_____ _____

C. Russell Philbrick
Professor of Electrical Engineering
Thesis Advisor

_____ _____

Jay S. Patel
Professor of Physics, Electrical Engineering
and Material Research

_____ _____

Daniel B. Lysak
Research Associate
ARL Remote Sensing Department

_____ _____

Larry C. Burton
Professor of Electrical Engineering
Head of the Department of Electrical Engineering

Abstract

An examination into the use of an Acousto-Optic Tunable Filter (AOTF) as a detection system for the lidar system has been made. The versatility of the AOTF and its ability to show accurate Raman scattering profiles of various species have been effectively demonstrated. The AOTF was used for spectroscopic applications and the results show that it could be applied to many new areas of spectroscopy. Attempts have been to made to successfully integrate the AOTF with the LAMP lidar system at Penn State to demonstrate a new capability to remotely detect and measure chemical species in the atmosphere. A lidar with a wavelength selection detector will provide an important way of monitoring plumes of pollutant species.

Table of Contents

List of Figures

List of Tables

Acknowledgments

I would like to thank my advisor Dr. Philbrick, for guiding me through my Masters program and helping me in becoming a successful researcher. My committee members, Dr. Lysak and Dr. Patel were quite supportive of my effort and gave valuable feedback.

Thanks are due to Franz Balsiger, Tom Petach, Glenn Pancoast, Bob Smith, Steve Esposito, Mike Zugger, Savya Mathur, and many other people without whose help and support I may not have achieved my objectives in this research effort.

Chapter 1

INTRODUCTION

Remote sensing for detection, and profiling of chemical species in the atmosphere has been a long term goal and promise of lidar techniques. There have been many efforts during the past twenty years which have contributed towards this goal. The application of laser remote sensing to measurement of atmospheric chemical species, whether they result from pollution sources, accidental release of hazardous vapor, from industrial processes, or from the release of toxic chemicals in the battlefield environment, is ready for major advances. The vibrational Raman scattering techniques can be effectively used for active remote sensing. Only techniques with high spectral resolution at optical wavelengths can provide the selectivity against interferents to monitor the chemical vapors in the background environment. The lidar design, in general, involves an elaborate optical configuration for the transmitter, and even more importantly, for the detection system. The use of Acousto-Optical Tunable Filters (AOTF) provides a special new capability for lidar detectors with flexibility to select the vibrational Raman line of interesting species. These devices are unique due to their compact size, frequency agility, ruggedness and high spectral resolution. Additionally, their frequency agility can be

used to select a wavelength to measure the concentration of any selected species in a smokestack plume.

1.1 Remote Sensing of Atmospheric Pollutants

Environmental pollution from industry and automobiles has developed into a global problem during the past few decades. While regulations are demanding strict emission standards from industries, increasingly sophisticated pollution monitoring techniques are being deployed. The main pollutant species of interest include NO_2, SO_2, and O_3. These species have considerable influence on health and it will be important to monitor these and other species continuously and accurately. The sources of some major pollution species and the health issues for them are listed in Table 1.1.

The Acousto-Optic Tunable Filter (AOTF), such as those designed by Prof. Pustovoit[1] that we are currently using at Penn State University, have some very interesting properties which make it useful for lidar remote sensing of atmospheric species [Pustovoit, 1994]. These devices have very high spectral resolution, about 0.2 nm at visible wavlength and good out of band rejection, order of 10^6. Wavelength selectivity is achieved by applying

---

[1]Vladislav I. Pustovoit; Professor, Corresponding member of the Russian Academy of Sciences; Director, Central design bureau for unique instrumentation; Deputy Director, Institute of Radioengineering and Electronics of the Russian Academy of Sciences.

a control signal which is an acoustic frequency signal and can be varied in real time if the source is controlled by a computer.

Table 1.1. Air Pollutants

Pollutant	Major Sources	Comments
Carbon Monoxide (CO)	automobile exhaust; Some industrial processes.	Health Standard: less than 9 ppm over 8hrs; less than 35 ppm over 1hr.
Sulfur Dioxide (SO_2)	Heat and power generation facilities that use oil or coal containing sulfur; sulfuric acid plants.	Health Standard: less than 0.03 ppm over a year; less than 0.14 ppm over 24 hrs.
Nitrogen Oxides (NO, NO_2)	Automobile exhaust; heat and power generation; explosives; fertilizer plants.	Health Standards: less than 0.05 ppm over a year for NO_2.
Photochemical oxidants (primarily ozone [O_3]; also peroxyacetyl nitrate [PAN] and aldehydes)	Formed in the atmosphere by the reaction of nitrogen oxides, hydrocarbons and sunlight.	Health Standards: less than 0.12ppm over 1 hr.

Chapter 2

PRINCIPLES OF AN AOTF

2.1 Introduction

The principle on which an AOTF device works is based entirely on optical scattering, whether we describe it later in terms of refractive index or scattering. Acousto-optic devices are based on the photoelastic effect by which an acoustic signal applied to a crystal produces a strain that changes the optical properties of the crystal. The acoustic signal is applied to the crystal by means of a piezoelectric transducer and as the acoustic wave propagates through the crystal, it produces regions of compression and rarefaction. The changes in the optical properties of the crystal are due to the changes in the scattering, that is the index of refraction, produced by the strain from the acoustic wave.

The photoelastic effect can be explained mathematically and it depends on the directional optical properties of the crystal lattice. It is described by a tensor relation between the elastic strain and the photoelastic coefficients [Goutzoulis, 1994],

$$\Delta B_{ij} = \Delta\left(\frac{1}{n^2}\right)_{ij} = p_{ijkl} S_{kl}, \qquad i,j,k,l = 1,2,3 \tag{2.1}$$

where ΔB_{ij} are the changes in the tensor component of the dielectric impermeability, $\Delta(1/n^2)_{ij}$ is the change in the $(1/n^2)_{ij}$ component of the optical index ellipsoid, p_{ijkl} is a fourth-rank photoelastic tensor, and S_{kl} are the strain components. The changes in the optical properties which are strain induced occur due to the changes in the index of refraction of the material. These optical changes are best described using the index ellipsoid to use as a model in calculating the difference in the ellipsoid equations for the perturbed and unperturbed states. Thus, an expression for the change in the index of refraction, as a function of the photoelastic coefficients and the strain, which is given by,

$$\Delta n_{ij} = 0.5 n_{ij}^3 p_{ijkl} S_{kl}, \qquad i,j,k,l = 1,2,3 \tag{2.2}$$

The crystal symmetry of any particular material determines which of the p_{ijkl} components are non zero and which components are related to others.

Acousto-optic interaction refers to the effect of the acoustic wave producing change in scattering properties on an incidental optical wave, because in most cases the presence of the optical wave does not change the optical properties of the crystal. Using the methods of classical optics, the AO interaction can be defined as the diffraction of the optical wave by a periodic phase grating induced by an acoustic wave. The fundamental difference between an ordinary grating and the phase grating is that the latter is not stationary and it travels with the speed of sound in the AO medium and its parameters can vary with time. This traveling phase grating

Doppler-shifts the optical frequency and the effect can be used to deflect, modulate or filter the optical beam. Although the design of these devices varies significantly, the underlying phenomenon are the same and is based on isotropic or anisotropic AO interactions.

2.2 Acousto-optic interactions

The characteristics of the diffracted light beam passing through an AO crystal can be determined by solving the wave equation that describes the optical wave propagation in the AO crystal. Diffraction spectra can be classified in two distinct diffraction regimes: Raman-Nath and Bragg diffraction.

At a given optical wavelength, at low acoustic frequencies or with a short interaction length (a short acoustic column), the propagation of the incident light in the interaction region remains rectilinear. The optical non-homogeneity of the medium, represented by the change in the refractive index, affects only the phase of the light transmitted through the acoustic column. As far as the optical interaction is concerned, the role played by the acoustic wave is to create a phase grating which has a periodic structure equal to that of the acoustic wave and which moves at the velocity of sound. This situation corresponds to Raman-Nath diffraction. Light diffraction in the Raman-Nath regime obeys the laws of diffraction by an ordinary phase grating, and thus we find symmetric equidistant

diffraction peaks. Figure 2.1 shows the basic geometry of the Raman-Nath interaction and the resulting multiple diffraction orders. The frequencies of the light in the diffraction peaks are also Doppler shifted by the moving phase grating.

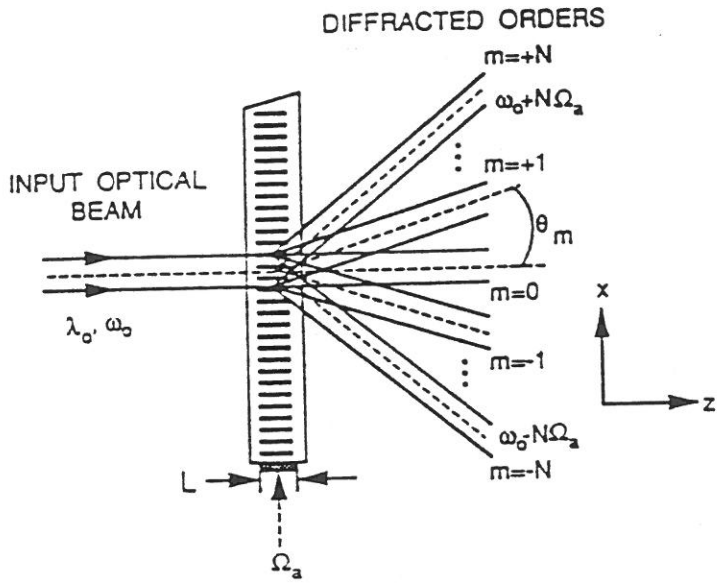

Figure 2.1. Raman-Nath acousto-optic diffraction geometry [Goutzoulis, 1994].

When the acoustic frequency or the length of the interaction region is increased beyond a certain point, the propagation of light in the acoustic column can no longer be considered rectilinear and the periodic structure which arises can no longer be regarded as a simple phase grating. The traversing light undergoes both amplitude and phase perturbations and there is a progressive transition from diffraction in the Raman-Nath regime to scattering by a three-dimensional periodic structure which corresponds

to the Bragg diffraction regime. In the transition region between the two diffraction regimes, the light incident at the Bragg angle gives rise to diffraction peaks of higher orders in addition to that of the first order. The angular positions of these peak with respect to the incident light remain the same as in Raman-Nath diffraction, but the intensity distribution becomes asymmetric. The first peak which is also called the Bragg peak is the most intense. As the frequencies and the depth of the acoustic field is increased further, the acousto-optic interaction becomes completely three-dimensional and there is a selective reflection of light at the Bragg angle from the moving periodic structure created by the acoustic wave. This situation corresponds to the Bragg diffraction regime. Figure 2.2 shows the basic geometry for the Bragg diffraction and the resulting single diffraction order. The effects of these two diffraction regimes on the acousto-optic interactions in isotropic and anisotropic mediums will be discussed in more detail in the following sections.

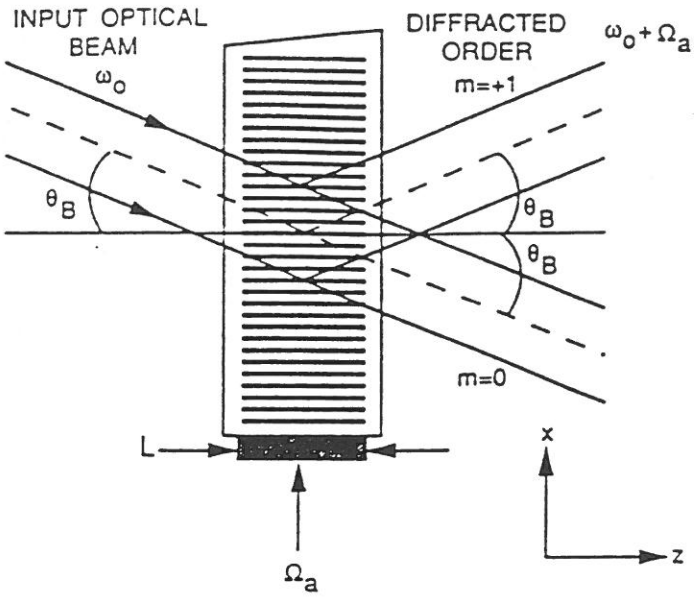

Figure 2.2. Bragg diffraction geometry [Goutzoulis, 1994].

2.2.1 Isotropic acousto-optic interactions

Isotropic acousto-optic interactions occur when the crystal used as the medium is isotropic (Raman, 1936). In this case the refractive indices for the incident and the diffracted optical beams are the same. In the case of isotropic interaction, as the acoustic wave propagates along the x axis and a plane optical beam propagates in the x-z plane at an angle θ_0 (inside the medium) from the z axis, the diffracted wave equation can be written as,

$$\nabla^2 E = \left[\frac{n(x,t)}{c}\right]^2 \frac{\partial^2 E}{\partial t^2}, \tag{2.3}$$

where $n(x,t)$ is the refractive index in the region of the AO interaction, c is the speed of light, and E is the electric field. The characteristics of the diffracted light beam can be determined by solving the wave equation.

When the acoustic wave is a planar, sinusoidal traveling wave, $n(x,t)$ can be described by,

$$n(x,t) = n + \Delta n \sin(\Omega_a t - K_a x), \tag{2.4}$$

where n is the average refractive index of the medium, Δn is the amplitude of the refractive index change due to the acoustic strain, K_a is the wave number of the acoustic wave and Ω_a is the frequency of the acoustic wave. The solutions of the wave equation cannot be expressed in an analytical form because $n(x,t)$ is periodic in both space and time. However, the perturbed optical field E can be expressed in a Fourier series expansion as,

$$\sum_{m=-\infty}^{\infty} E_m(z) e^{j[(\omega_i + m\Omega_a)t - k_m \bullet r]}, \tag{2.5}$$

where,

$$k_m \bullet r = k_i(z \cos\theta_0 - x \sin\theta_0) + mK_a x, \tag{2.6}$$

where E_m and k_m are the amplitude and the wave vector of the mth diffracted light beam respectively, and ω_i and k_i are the frequency and the wave number of the incident light respectively. Equations (2.5) and (2.6) represent an expansion in plane waves of the output light distribution from which the frequency of the $\pm m$th diffracted order, ω_{dm}, can be expressed as,

$$\omega_{dm} = \omega_i \pm m\Omega_a. \tag{2.7}$$

The above equation implies that the optical frequency of the mth diffracted order will be shifted by an amount equal to the frequency of the mth harmonic of the acoustic signal. Using Equations (2.3), (2.4), (2.5) and

(2.6), a set of coupled-wave equations can be derived which describe the interaction of the optical and the acoustic waves in AO medium (Raman, 1936),

$$\frac{dE_m}{dz} + \frac{u_1}{2L}(E_{m+1} - E_{m-1}) = j\frac{mK_a}{\cos\theta_0}\left[\frac{mK_a}{2k_i} - \sin\theta_0\right]E_m , \qquad (2.8)$$

where,

$$u_1 = \frac{-k_0 \Delta n L}{\cos\theta_0} , \qquad (2.9)$$

and $k_0 = 2\pi/\lambda_0$ is the wave number of the incident optical beam in free space and λ_0 is the optical wavelength in free space. As different optical waves propagate in the AO crystal an energy exchange takes place between them. Equation (2.8) can be interpreted by applying basic coupled-mode theory (Kogelnik, 1969). If the acoustic waves are sinusoidal, then the optical waves can exchange energy only with the adjacent waves. The variable u_1 is viewed as the coupling constant between the adjacent waves. The amount of energy depends on the coupling constant and the degree of synchronization (which is a measure of the phase difference) of the waves. This is given by the factor ($m^2K^2{}_a/2k_i \cos\theta_0$), which forms the right side of Equation (2.8). A larger the value for this factor, corresponds to a smaller degree of synchronization, that is, the larger phase difference between the waves corresponding to a smaller amount of energy transferred.

The mechanical arrangement and geometry of the AO interaction also affect the energy transfer. The Klein and Cook parameter (Klein, 1967) is used to determine the amount of light that can be transferred from the zero order to the diffracted orders. This parameter which is denoted by Q is given by the relation,

$$Q = \frac{K_a^2 L}{k_i \cos\theta_0} = \frac{2\pi\lambda_0 L}{n\Lambda^2 \cos\theta_0}, \tag{2.10}$$

where L is the AO interaction length along the direction of propagation of light and Λ is the wavelength of the acoustic wave. Incorporating the factor Q in Equation (2.8), we have,

$$\frac{dE_m}{dz} + \frac{u_1}{2L}(E_{m+1} - E_{m-1}) = j\left[\frac{m^2 Q}{2L} - mK_a \tan\theta_0\right]E_m. \tag{2.11}$$

Equation (2.11) shows that an appreciable amount of energy can be transferred out of the zero order if either or both of the coefficients on the right side of the equation are small for $m = \pm 1$. This can be true only if Q is small and θ_0 is close to 0° or if the two terms are equal and Q is large.

As we will see shortly, the case when Q is small corresponds to Raman-Nath diffraction and the case when Q is large and the two terms equal corresponds to Bragg diffraction. The value of Q also determines the diffraction pattern which occurs due to the AO interaction. For values of $Q \leq 0.3$, the AO diffraction is from the Raman-Nath regime and exhibits the diffraction pattern as shown in Figure 2.1. In this case the light is

transferred from the zeroth order to the first order, from the first order to the second order and so on. The angle θ_m represents the angle between the mth diffracted order and that of the undiffracted order which is the principal optical beam. The diffraction angle can be approximated as,

$$\theta_m = \pm\frac{m\lambda_0}{n\Lambda}. \tag{2.12}$$

Since the value of Q in this case is less than 0.3, Equation (2.11) can be simplified by neglecting the first term on the right side and by applying the boundary conditions, $E_0(0) = E_0$ and $E_m(0) = 0$, yields,

$$E_m(z) = E_0 e^{-jmX} J_m\left\{\frac{2u_i \sin X}{K_a L \tan\theta_0}\right\}, \tag{2.13}$$

where $X = (K_a z \tan \theta_0)/2$ and J_m is the Bessel function of the mth order. The normalized intensity (I_m/I_0) of the mth diffracted order at $z = L$ can be expressed as

$$I_d^m = J_m^2\left\{u_1 \frac{\sin((K_a L \tan\theta_0)/2)}{(K_a L \tan\theta_0)/2}\right\}. \tag{2.14}$$

It can be seen that the diffraction pattern is symmetric for all angles of incidence.

For values of Q greater than 7, the acoustic grating is no longer thin and the diffraction regime is called Bragg. Since energy transfer is most effective between optical waves with the same phase term, the diffracted light appears predominantly as a single order, such as that illustrated in Figure 2.2. The amount of light in the diffraction order is maximized when

the terms on the right side of Equation (2.11) are equal. Then tan θ_0 = $mQ/2K_aL$. For m = 1, this condition reduces to,

$$\sin\theta_0 = \sin\theta_B = \frac{K_a}{2k_i} = \frac{\lambda_0}{2n\Lambda}, \tag{2.15}$$

where θ_b is called the Bragg angle. It is usually of the order of a few degrees.

The Bragg interaction can also be explained by collision theory where the scattering occurs between a photon and a phonon. Applying the laws of conservation of energy and momentum, the collision results in a new photon which is at a different frequency and with different momentum. The frequency and momentum relations for the collision can be mathematically represented as

$$\omega_d = \omega_i \pm \Omega_a \tag{2.16}$$

and

$$k_d = k_i \pm K_a \,, \tag{2.17}$$

where ω_d and k_d are the frequency and wave number of the resulting photon, ω_i and k_i are the frequency and wave number of the incident photon, Ω_a and K_a are the frequency and wave number of the scattering phonon. The resulting frequency of the photon can be greater or lesser than that of the initial photon depending on whether the optical wave is moving against or with the acoustic wave. These equations clearly show that the

diffracted optical beam is Doppler shifted and that it could be shifted either up or down. Since the value of ω_i far exceeds that of Ω_a, the magnitude of k_d is approximately that of k_i. Hence, the diffraction triangle in the wave vector diagram is isosceles and this is illustrated in Figure 2.3. From the Figure 2.3, we can see that the magnitude of K_a is $2|k_i|$ sin θ_B, which is the expression in Equation (2.15). We also note that when the Bragg condition is satisfied, the angle between the incident and the diffracted beams is $2\theta_B$. Another point of interest is that the wave vectors lie on one circle for isotropic interactions, because the refractive indices for the incident and the diffracted beams are equal.

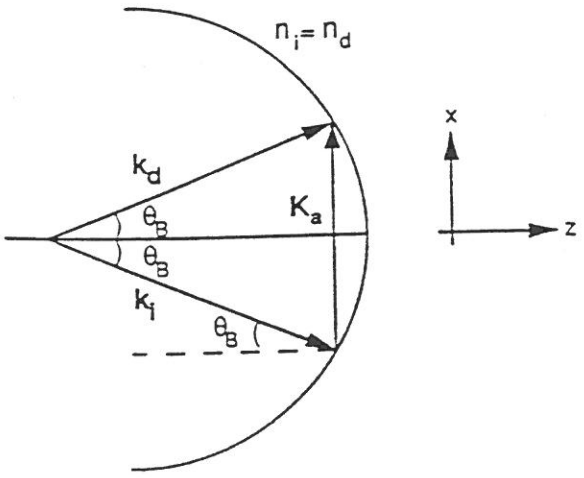

Figure 2.3. Wave vector diagram for isotropic Bragg diffraction.

In order to deduce an expression for the normalized intensity, assume ideal isotropic Bragg diffraction where energy transfer occurs only

between the incident optical wave E_0 and the diffracted optical beam E_1. When θ_0 is almost equal to θ_B, Equation (2.11) reduces to,

$$\frac{dE_0}{dz} + \frac{u_1}{2L}E_1 = 0, \tag{2.18}$$

and,

$$\frac{dE_1}{dz} - \frac{u_1}{2L}E_0 = j\frac{2q}{L}E_1, \tag{2.19}$$

where,

$$q = \frac{K_a L \sin\theta_B}{2\cos\theta_0} - \frac{K_a L \tan\theta_0}{2}. \tag{2.20}$$

On solving the differential Equations (2.18) and (2.19) (Phariseau, 1956), the normalized intensity of the diffracted beam, I_d, can be calculated by setting $z = L$ [Goutzoulis, 1994], yielding,

$$I_d = \left[\frac{u_1}{2}\right]^2 \frac{\sin^2\left[\sqrt{(q^2 + (u_1/2)^2)}\right]}{q^2 + (u_1/2)^2}. \tag{2.21}$$

When the Bragg condition is satisfied, $\theta_0 = \theta_B$, $q = 0$ and the diffracted beam intensity is maximized and described by,

$$I_{dm} = \sin^2\left[\frac{u_1}{2}\right]. \tag{2.22}$$

Thus Equation (2.14) represents the normalized diffraction beam intensity for an isotropic acousto-optic interaction in the Raman-Nath diffraction regime and Equation (2.22) represents the normalized intensity in the Bragg diffraction regime. For normal incidence, Equation (2.14)

reduces to $I_d^m = J_m^2(u_1)$, and since for $m = 1$ the maximum value of $J_1(u_1) = 0.58$, the maximum normalized diffracted beam intensity is 33.6%. The term "diffraction efficiency" is also used to denote the normalized diffracted beam intensity. While in the case of Bragg diffraction, for $u_1 = \pi$, the normalized intensity is equal to 1, and hence a diffraction efficiency of 100% is obtained. Thus the usefulness of Raman-Nath acousto-optic devices is restricted by the limited diffraction efficiency due to the appearance of multiple diffracted orders.

The input acoustic power input P_a can be expresses in terms of strain and other physical parameters of the crystal (Smith, et al, 1965) and is given by,

$$P_a = 0.5\rho V^3 S_{kl} S_{kl}^* LH, \tag{2.23}$$

where ρ is the density of the AO crystal, V is the acoustic wave velocity, and H is the height of the acoustic beam. Using Equations (2.2), (2.9) and (2.23), an expression for the parameter u_1 can be obtained in terms of the physical parameters for AO interaction,

$$u_1 = \frac{2\pi}{\lambda_0 \cos\theta_0}\left(\frac{n^6 p^2}{\rho V^3}\right)^{1/2}\left(\frac{P_a L}{2H}\right)^{1/2}. \tag{2.24}$$

Substituting for u_1 in Equation (2.22),

$$I_{dm} = \sin^2\left\{\frac{\pi}{\lambda_0 \cos\theta_0}\left(\frac{n^5 p^2}{\rho V^3}\right)^{1/2}\left(\frac{P_a L}{2H}\right)^{1/2}\right\}. \tag{2.25}$$

Thus, we have an expression for the normalized diffracted beam intensity which is related to the physical and geometrical characteristics of an acousto-optic device and the input acoustic power. As stated before, this normalized intensity is also called diffraction efficiency and is denoted by η and is expressed in percent per watt of the applied acoustic power P_a. Equation (2.25) can be approximated for small values of u_I as,

$$\eta \cong \frac{\pi^2}{2\lambda_0^2 \cos^2\theta_0}\left(\frac{n^6 p^2}{\rho V^3}\right)\left(\frac{P_a L}{H}\right). \tag{2.26}$$

Another useful term generally used in context to acousto-optic devices is called the figure of merit,

$$M_2 = \frac{n^6 p^2}{\rho V^3}. \tag{2.27}$$

M_2 is a figure of merit which determines the inherent efficiency of the acousto-optic material regardless of the interaction geometry. The equation shows that for high efficiency, materials must have a high index of refraction and a low acoustic velocity. M_2 is mainly used to describe AOTFs and also some scanners and low bandwidth, high resolution deflectors.

The 3-dB AO bandwidth parameter, Δf, defined as the difference between the highest and the lowest frequencies at which the normalized diffracted intensity I_d drops by 50%, is useful for practical Bragg diffraction based devices. It is given by the following expression,

$$\Delta f = 1.8nV^2 \frac{\cos\theta_0}{\lambda_0 L f_c}. \tag{2.28}$$

It can be seen that the 3-dB bandwidth is inversely proportional to the interaction length, L. But on the other hand, efficiency is proportional to L (Equation 2.26), and hence there is a bandwidth-efficiency trade-off.

2.2.2 Anisotropic Acousto-optic interactions

Anisotropic AO interactions occur in crystals which are optically anisotropic and involve diffraction between ordinary and extraordinary optical beams. This AO interaction, also called as birefringent AO interaction results in the diffracted and incident beams have orthogonal polarization. This is property could be used in filtering and reducing the optical noise and to separate the diffracted and un-diffracted beams by using a polarizer.

Figure 2.4 shows the wave vector diagram for the birefringent diffraction in a negative uniaxial crystal where $n_o > n_e$. In a birefringent crystal, the diffracted light wave vector k_d can differ in magnitude from k_i if the polarization is changed during the scattering interaction.

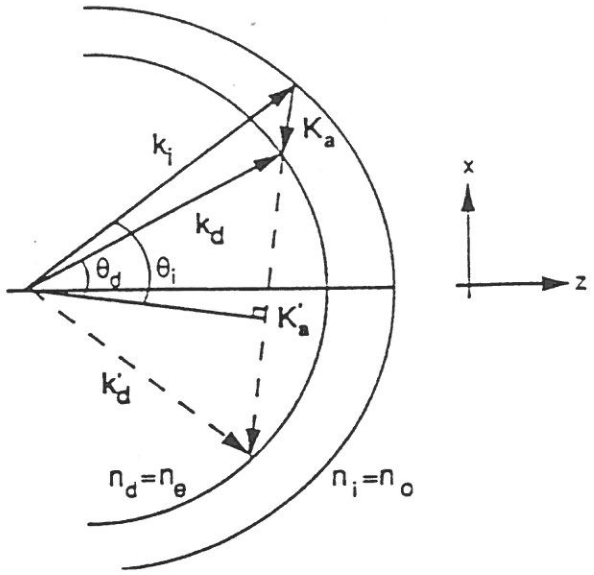

Figure 2.4. Wave vector diagram for the general case of anisotropic diffraction [Goutzoulis, 1994].

For a given acoustic direction, there exist two distinct acoustic frequencies which satisfy the exact momentum matching conditions. It can be seen from Figure 2.4 that a change in direction of the diffracted wave vector k_d to k_d' can be achieved by a change in the magnitude of the acoustic wave vector K_a to K_a'. Thus an optical beam can be deflected simply by varying the frequency of the a well collimated acoustic beam which remains fixed in direction. This means that the angular spread of the acoustic wave vector required for phase matching across a particular acoustic bandwidth needs to be much smaller for an anisotropic interaction than for the isotropic interaction. Thus AO devices with much wider bandwidths (for fixed diffraction efficiency) or with much higher diffraction efficiencies (for fixed bandwidth) can be designed.

To obtain the normalized diffracted beam intensity, an approach (Chang, 1976) similar to the one described in the previous section is followed. The coupled wave equation is obtained (Goutzoulis, 1994) and is given by the following expression,

$$\frac{dE_0}{dz} = j\frac{k_i n_d^2 p S^*}{4\cos\theta_0} E_1, \tag{2.29}$$

where S is the strain of the acoustic wave and p is the appropriate photoelastic coefficient. Similarly, the first order coupled wave equation is found to be,

$$\frac{dE_1}{dz} - j\Delta K_1 E_1 = j\frac{k_1^2 n_1^2 p S}{4k_i c_1} E_0, \tag{2.30}$$

where ΔK_1 is the magnitude of momentum mismatch for the first order, $c_1 = \cos\theta_0 + (K_a/k_i)\cos\theta_a$, and n_1 is the refractive index.

Equations (2.29) and (2.30) are similar to Equations (2.18) and (2.19) and hence their solutions are similar. Therefore, the normalized intensity of the first diffracted order has a $(\text{sinc})^2$ type profile given by the expression in Equation (2.21). However, in the case of anisotropic interaction the value of variables q and u_1 are different,

$$q = \frac{\Delta K_1 L}{2}. \tag{2.31}$$

$$\left(\frac{u_1}{2}\right)^2 = \frac{\pi^2 n_i^3 n_d^3 p^2 |S|^2 L^2}{4\lambda_0^2}. \tag{2.32}$$

The normalized anisotropic diffraction efficiency is calculated , for small values of $u_1$using the same procedure as the previous section,

$$\eta_a \cong \frac{\pi^2}{2\lambda_o^2}\left(\frac{n_i^3 n_d^3 p^2}{\rho V^3}\right)\left(\frac{P_a L}{H}\right). \tag{2.33}$$

Comparing Equations (2.26) and (2.33), we see that the expression for diffraction efficiency for both isotropic and anisotropic interaction are very similar. Instead of the n^6 parameter in the isotropic case, we have a $n_i^3 n_d^3$ term for the anisotropic case. Therefore, the anisotropic figure of merit, M_{2a}, is given by,

$$M_{2a} = \frac{n_i^3 n_d^3 p^2}{\rho V^3}. \tag{2.34}$$

Since the factor q is quite different for the isotropic and anisotropic Bragg interactions, substantially different bandwidths are found for a given interaction length. The 3-dB bandwidth expression [Goutzoulis, 1994] is given by,

$$(\Delta f_a)^2 = \frac{3.6 n_i V^2 \cos\theta_0}{L_a \lambda_0}. \tag{2.35}$$

Equation (2.35) describes the bandwidth relationship for an anisotropic AO interaction for the interaction length L_a. By comparing Equation (2.28) with Equation (2.35), a relationship between anisotropic bandwidth, Δf_a, and the isotropic bandwidth, Δf_i, can be determined,

$$(\Delta f_a)^2 = 2 f_c \Delta f_i \tag{2.36}$$

Equation 2.36 shows that for the case of same interaction length, anisotropic interaction has a significant bandwidth advantage over the isotropic case. The larger effect is due to the change in the Bragg angle around the center frequency being much smaller in anisotropic compared to isotropic diffraction. The bandwidth advantage also translates into larger effective interaction lengths for the anisotropic diffraction.

In anisotropic AO crystals, two diffraction geometries are possible. An ordinarily polarized k_i will result in an extraordinarily polarized k_d and an extraordinarily polarized k_i will result in an ordinarily polarized k_d. In both cases, the frequency of the diffracted beam can be shifted up or down depending on (a) the type of crystal used (positive or negative), and (b) the direction of the acoustic wave. The polarization rotation makes multiple diffraction impossible and hence diffraction from the Raman-Nath regime cannot occur in anisotropic media.

The general description of anisotropic diffraction has two limiting cases. We see from Figure 2.4 that when collinear anisotropic interaction occurs, k_i, k_d and K_a propagate in the same direction, there exists a lower critical frequency f_{min} below which Bragg diffraction cannot occur. This frequency is given by,

$$f_k = (n_i - n_d)\frac{V}{\lambda_0} = \frac{V\Delta n}{\lambda_0}. \qquad (2.37)$$

This condition is of great importance for AOTFs because it describes the phase matching conditions for a given acoustic frequency over a wide range of incident light directions, thus allowing larger angular apertures. The second case involves the degeneration of the two matching solutions, referred to as tangential or (90°) birefringent phase matching. Here, K_a is tangential to the inner circle in Figure 2.4, and phase matching can take place over a wide range of acoustic frequencies because the direction of K_a does not have a sharp dependence on the acoustic frequency changes.

2.3 Classification and selection of AOTF types

Acousto-Optic interactions are used to broadly classify AO devices as isotropic and anisotropic devices depending upon the crystal properties. They are also classified on the basis of the diffraction regimes as Raman-Nath and Bragg diffraction. These classifications have been thoroughly discussed in the preceding sections.

In principle, both isotropic and anisotropic Bragg diffraction can be used for spectral filtering. However, a filter based on isotropic diffraction is impractical because its optical passband is dependent upon the angular aperture of the incident beam and is only usable with a well collimated light (of the order of milliradians). The angular aperture limitation arises because a change in the angle of the incident light will introduce a momentum mismatch. For an incident light beam of finite divergence, the

width of the passband is greatly increased. In addition, the diffracted beam is deflected to a different angle for each wavelength. Therefore, the design of an AOTF is based on anisotropic Bragg diffraction in a birefringent crystal. This diffraction involves a rotation of the polarization plane of the diffracted wave. Due to the birefringence property, it is possible to chose the direction of the acoustic wave propagation so that the group velocity for both the incident and the diffracted light is collinear. This process is referred to as non-critical phase matching (NPM). Under the NPM condition [Dixon, 1967], maximum compensation of the momentum mismatch due to the angular deviation of the incident light beam is achieved by the angular change of the birefringence ($\Delta n = n_i - n_d$). Hence, the NPM is maintained to the first order over a large angular change of the incident light beam and this property is used in the design of non-collinear AOTFs.

AOTF devices fall into two categories in terms of configurations: collinear and non-collinear AOTFs. In a collinear AOTF, the incident light, the diffracted filtered light and the acoustic wave all interact collinearly in a birefringent crystal. In this configuration, the polarization of the incident and the diffracted beams are orthogonal and since they are collinear, a polarizer is used to separate them. In a non-collinear AOTF [Goutzoulis, 1994], the acoustic and the optical waves propagate at quite different angles through the crystal. In this configuration, polarizers need not be

necessarily used for separating the zero-order and the diffracted beams. It is possible to extract the filtered beam by spatial separation provided the angular divergence of the input beam is not larger than the angular separation between the zero and the first diffracted order. Thus both polarizations of the selected wavelength can be obtained simultaneously. This is an useful feature in some applications, such as polarimetry. When the input beam divergence is larger than angular separation of the orders, the filtered beam must be separated using a high rejection polarizer, else the unfiltered optical power may be orders of magnitude higher than the filtered and hence degrade the signal-to-noise ratio.

Hence, for well a collimated input beam, a collinear AOTF can be used for spectral filtering, while a non-collinear AOTF is more suited for input beams with large divergence and for applications in spectral imaging.

2.4 Materials used for AOTFs

The list of crystals available for use in AOTFs is restricted by the symmetry requirements on the photoelastic tensor [Goutzoulis, 1994]. The preferred characteristics of the crystal material include (a) high optical transmission over the desired spectral range, (b) high uniformity, (c) low scattering, (d) low acoustic losses, (e) reasonably high AO figure of merit, and (f) suitable mechanical properties so that the crystal can be cut,

polished and bonded with ease to the transducers. Some of the commonly used materials and their important properties are shown in Table 2.1.

The only crystal available for wavelengths into the far UV is α-quartz, which can used for both collinear and non-collinear designs. It is an excellent optical and acoustical material, is inexpensive and available in very large sizes. However, its AO figure of merit is poor and hence requires very high RF input powers. Because of the quadratic dependence of power on wavelength, its usefulness is limited to the shorter wavelengths. Crystals available for the visible and IR to about 4 μm include lithium niobate ($LiNbO_3$) and calcium molybdate ($CaMoO_4$) for collinear AOTFs, and tellurium dioxide (TeO_2) as the material of choice for non-collinear AOTFs. TeO_2 is a popular choice for commercial AOTFs and is optically active, as is α-quartz, a property which has impact on certain AOTF designs in which the light is incident at angles near the crystal optic axis.

Table 2.1. Properties of AOTF crystals [Goutzoulis, 1994]

Crystal	Transmission range (μm)	Refractive indices	Acoustic velocity ($x10^5$cm/sec)	AO figure of merit (relative to SiO_2)	AOTF type
α-quartz	0.12-4.5	n_o = 1.539 n_e = 1.548	6.32	1	Collinear or non-collinear
$LiNbO_3$	0.4-4.5	n_o = 2.23 n_e = 2.15	6.57	4.6	Collinear
$CaMoO_4$	0.4-4.5	n_o = 1.95 n_e = 1.96	6.0	14	Collinear
TeO_2	0.35-4.5	n_o = 2.26 n_e = 2.41	0.62	79	Non-collinear
TI_3AsSe_3	1.25-17	n_o = 3.38 n_e = 3.19	1.0	500	Collinear or non-collinear
Hg_2Cl_2	0.4-20	n_o = 1.9 n_e = 2.4	0.35	700	Non-collinear
TI_3Pse_4	0.85-8.5	n_o = 2.765 n_e = 2.798	2.0	1350	Non-collinear

Chapter 3

RAMAN SPECTROSCOPY USING AN AOTF

3.1 Elastic and Inelastic Scattering

The spontaneous emission of a photon of radiant energy by an excited atom is regarded as a first-order radiative process, whereas the scattering of electromagnetic energy by a molecule (or atom) is regarded as a second order interaction, since two photons are involved. A photon of the incident radiation is annihilated while a photon of scattered radiation is created. The scattering is said to be elastic if the scattered frequency is the same as the incident frequency, and this form of scattering is generally termed as Rayleigh scattering. The Rayleigh scattering cross-section is considered to include the thermal Doppler spread and the rotational Raman states of the scattering molecules. If there is a change in the frequency, the scattering is termed as inelastic and the energy difference associated with the scattering is observed in a change in the quantum state of the scattering particle, such as the vibrational Raman scattering.

Consider the interaction of an electromagnetic wave, $E = E_0 \cos \omega t$, with an atomic system that has a polarizability,

$$\psi(x,t) = \psi_{x=0} + \left(\partial\psi / \partial x\right)_{x=0} x + \ldots, \tag{3.1}$$

where x is the charge displacement from equilibrium, $(x=0)$, $\psi_{x=0}$ represents the equilibrium polarizability, and $\left(\partial\psi/\partial x\right)_{x=0}$ represents the field induced polarizability. If the atomic system can be treated as a simple harmonic oscillator with angular frequency ω_1, then $x = x_0 \cos \omega_1 t$, and the polarization of the atomic system becomes,

$$\psi(x,t) = \left\{\psi + \left(\frac{\partial\psi}{\partial x}\right)_{x=0} x\right\} E_0 \cos\omega t\,, \tag{3.2}$$

which gives,

$$\psi(x,t) = \psi_{x=0} E_0 \cos\omega t + \frac{1}{2} E_0 x_0 \left(\frac{\partial\psi}{\partial x}\right)_{x=0} \left\{\cos\left(\omega+\omega_1\right)t + \cos\left(\omega-\omega_1\right)t\right\}. \tag{3.3}$$

It can be seen that if $\left(\partial\psi/\partial x\right)_{x=0} = 0$, then there is no inelastic scattering. Consequently, it is the oscillating polarizability that can be thought of as modulating the scattered radiation and thereby leading to the appearance of the three frequencies ω, $\omega + \omega_1$, $\omega - \omega_1$. The first corresponds to Rayleigh scattering, the second to Raman anti-Stokes scattering, and the third to Raman Stokes scattering. The Stokes and anti-Stokes scattering processes are schematically illustrated in Figure 3.1. The figure illustrates the occurrence of the first few orders of Stokes and anti-Stokes lines. Higher orders of the Stokes lines depend upon the energy transfer from the virtual state to higher order vibrational states.

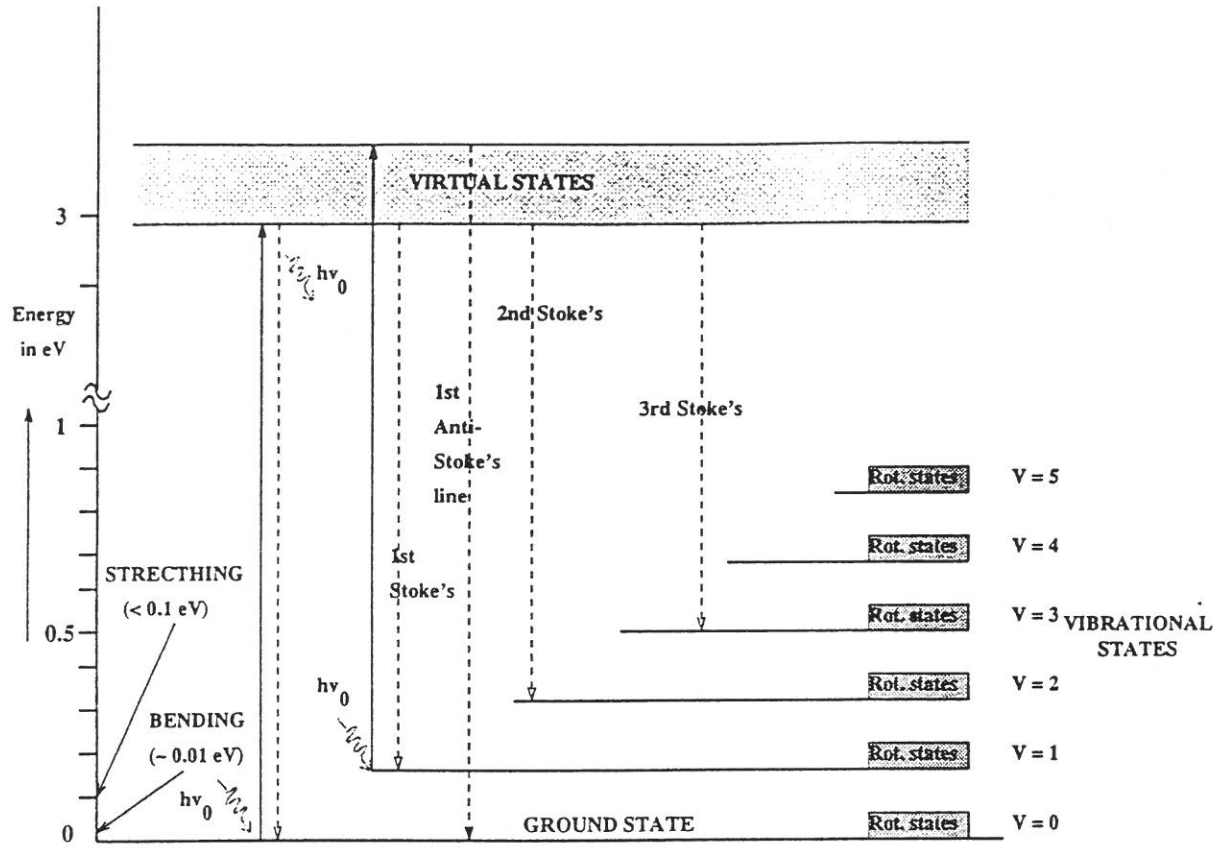

Figure 3.1. Schematic representation of vibrational Raman scattering.

At ambient temperature, most simple molecules are in their vibrational ground state. According to Boltzmann's law, a much smaller number of the molecules are in the vibrationally excited states. Therefore, the Raman scattering which transfers vibrational energy to the molecules and scatters quanta of lower energy (Stokes lines) has a higher probability of occurrence than the reverse scattering process (anti-Stokes lines). Hence Stokes lines are of higher intensity than the anti-Stokes lines.

However, larger molecules with more degrees of freedom have smaller energy decrements between states and thus, some of the larger molecules do have significant anti-Stokes scattering at room temperature.

The structure of the Raman spectrum is quite complex. The intensity of the spectral lines depends not only on the electronic transition probabilities, selection rules, and the frequency, but also on the number of molecules in the initial state [Herzberg, 1950]. A spectral analysis of the scattered light reveals the existence of a series of lines at up and down shifted side-band frequencies which correspond to the vibrational-rotational frequencies of the molecules irradiated.

3.2 Vibrational Raman Spectra

Vibrational spectra contain information about every aspect of molecular structure. This information can be evaluated by comparing observed Raman spectra with those calculated from systematically derived models. Much research has been done in predicting the spectra of various molecular species, these results can be traced back to the early days of vibrational spectroscopy [Herzberg, 1950; Kohlrausch, 1938; Schrader, 1968].

Those vibrations which change bond lengths are called stretching vibrations and those which change bond angles are bending and torsional

hand, are generally composed of only certain different kinds of atoms connected by a few different types of bonds. The great variety of organic compounds leads to the possibilities of combining the basic arrangements of molecules into different constituents, configuration, size and substitution pattern. Hence, complex molecules may be characterized by vibrations of definite frequency modified by definite interaction pattern. These vibrations, often referred to as the characteristic vibrations, are especially useful in the study of organic compounds.

The vibrational spectrum of organic compounds could be divided into a few typical regions:

(i) The X-H stretching vibrations, where X denotes atoms of typical organic molecules like C, O, N, S, and the halogens, are typically located in the frequencies between 3700 and 2500 cm^{-1}.

(ii) The region between 2500 and 2000 cm^{-1} exhibits stretching vibrations of groups with triple bonds as well as the anti-symmetric stretching vibrations of groups with cumulated double bonds, X=Y=Z, where X, Y and Z could represent C, O, N, S, and the halogens.

(iii) The stretching vibrations of double bonded X=Y groups are in the region between 2000 and 1500 cm^{-1}.

(iv) The deformation vibrations of the X-H groups are seen in the region between 1500 and 1000 cm^{-1}.

(v) In the region between 1300 and 600 cm $^{-1}$, the stretching vibrations of single bonds of atoms of the second period can be seen.

(vi) The region between 600 and 200 cm^{-1} shows the bending vibrations of the above group and stretching vibrations of groups with heavier atoms.

(vii) Finally, between 200 and 20 cm $^{-1}$, the lattice vibrations of crystalline molecules are found.

Table 3.1 shows the characteristic frequencies and the intensity strengths for both the Raman and infrared scattering in organic compounds.

Table 3.1 Characteristic frequencies with Raman and infrared intensities of groups in organic compounds.

Vibration	Region (cm^{-1})	Intensity	
		Raman	Infrared
ν(O-H)	3650-3000	w	s
ν(N-H)	3500-3300	m	m
ν(≡C-H)	3300	w	s
ν(=C-H)	3100-3000	s	m
ν(-C-H)	3000-2800	s	s
ν(-S-H)	2600-2550	s	w
ν(C≡N)	2255-2220	m-s	s-0
ν(C≡C)	2250-2100	vs	w-0
ν(C=O)	1820-1680	s-w	vs
ν(C=C)	1900-1500	vs-m	0-w
ν(C=N)	1680-1610	s	m
ν(N=N)	1580-1410	m	0

$\nu_a((C-)NO_2)$	1590-1530	m	s
$\nu_s((C-)NO_2)$	1380-1340	vs	m
$\nu_a((C-)SO_2(-C))$			
$\nu_s((C-)SO_2(-C))$	1350-1310	w-0	s
$\nu((C-)SO(-C))$	1160-1120	s	s
$\nu(C=S)$	1070-1020	m	s
$\delta(CH_2)$, $\delta_a(CH_3)$	1250-1000	s	w
$\nu(CC)$, aromatics	1470-1400	m	m
$\nu(CC)$, alicyclics	1600-1500	s-m	m-s
$\nu_a(C-O-C)$	1300-600	s-m	m-w
$V_s(C-O-C)$	1150-1060	w	s
$\nu_a(Si-O-Si)$	970-800	s-m	w-0
$\nu_s(Si-O-Si)$	1110-1000	w-0	vs
$\nu(O-O)$	550-450	vs	w-0
$\nu(S-S)$	900-845	s	0-w
$\nu(C-Cl)$	550-430	s	0-w
$\nu(C-Br)$	800-550	s	s
$\nu(C-I)$	700-500	s	s
Lattice vibrations in molecular crystals	660-480	s	s
	200-20	vs-0	s-0

ν- stretching vibration, δ- bending vibration, ν_s- symmetric vibration, ν_a- anti-symmetric vibration.

vs- very strong, s- strong, m- medium, w- weak, 0- very weak or inactive

3.3 Experimental observations of vibrational spectra using AOTF

The use of the Acousto-Optic Tunable Filter (AOTF) as a detector for spectroscopic applications has been investigated by applying it to make several measurements. Experiments were carried out the Penn State Lidar lab that use an AOTF for obtaining Raman spectra of molecular vibrations. Samples of various organic compounds were excited using a laser and the scattered light was studied with the AOTF. This section summarizes the research work done.

3.3.1 Experimental Setup

The spectroscopic experiments were done on an optical bench and the layout is shown in Figure 3.2. The excitation source used was an Argon-ion CW laser with a peak output of 1.1 Watts at the 514.5 nm laser wavelength. The laser was tuned to its peak output power. The chemical sample was stored in a cylindrical quartz cuvette with an approximate capacity of 50 ml. An energy monitor was used to monitor the power output of the laser and it also served as a beam stop. The laser beam was directed perpendicular to the front face of the cylindrical cuvette and the scattered light collected perpendicular to the beam. The cylindrical cuvette also acted as a positive lens for the scattered light.

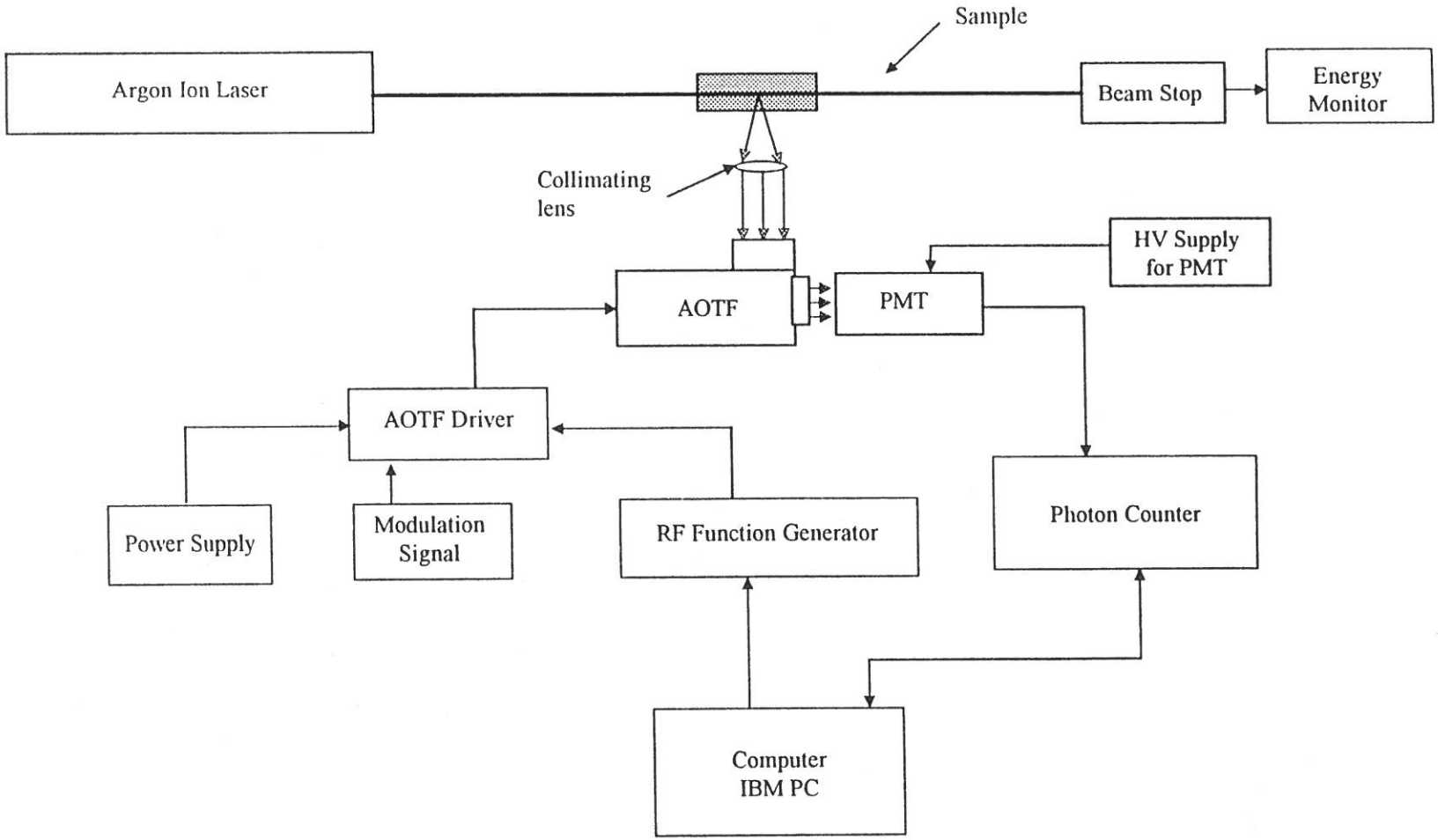

Figure 3.2 Experimental set up to determine the Raman scattering profiles of various samples using the AOTF.

The Raman scattered light, due to both the vibrational mode and the stretch mode of the molecules, is collected using a collimating lens arrangement and formed into a beam for passing through the AOTF and a blocking filter for the laser light. The AOTF is driven by circuitry which uses an RF control signal for wavelength selection. The optical output signal from the AOTF strikes the Photo Multiplier Tube (PMT) and the signal from the PMT is measured using a SR-430 Multi-channel scaler/averager. The RF signal is generated by a HP8656A Function Generator which is controlled by an IBM PC through a GPIB interface. The photon counter is controlled through a RS232-C serial interface. The modulation signal is generated at a duty cycle of 1/3 which, was recommended to reduce the average RF power to modulate the AOTF. The triggering of the photon counter and the modulation signal are synchronized to ensure proper counting. The AOTF has a finite acoustic transit time for the modulation signal coupled with the acoustic signal to set up the phase grating within the length of the crystal at the speed of sound in the material, which is about 50 μs. The photon counter is delayed so that the counting starts corresponding to the AOTF set up time. The computer collects the data from the photon counter. For every preset frequency, data from the photon counter is collected both during the time when the modulating signal is high as well as when it is low.

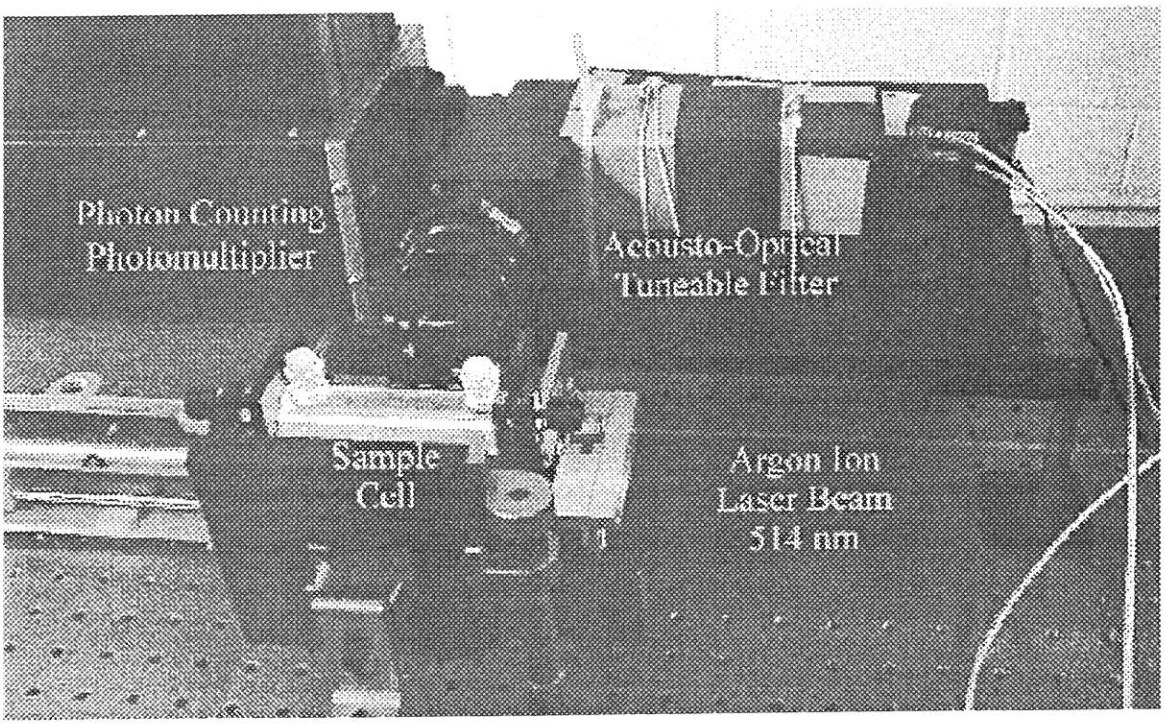

Figure 3.3 AOTF being used for vibrational spectroscopy on an optical bench.

Figure 3.3 shows an experiment using the AOTF being conducted on an optical bench. The software which controls the apparatus was written in QBASIC. The data set, which included the frequency, total counts, mean and deviation of the counts during both the modulation periods, is stored in a file.

3.3.2 Configuring the AOTF

The AOTF used in this research work was developed by Prof. Vladislav I. Putovoit . The specifications of the device is listed below.

Specifications:

(i) Crystal	Quartz (SiO_2)
(ii) Spectral range	400-800 nm
(iii) Control signal range	65-120 MHz
(iv) Spectral resolution	0.2 nm
(v) Entrance angular aperture	2.0 degrees
(vi) Polarizer	Calcite ($CaCO_3$)

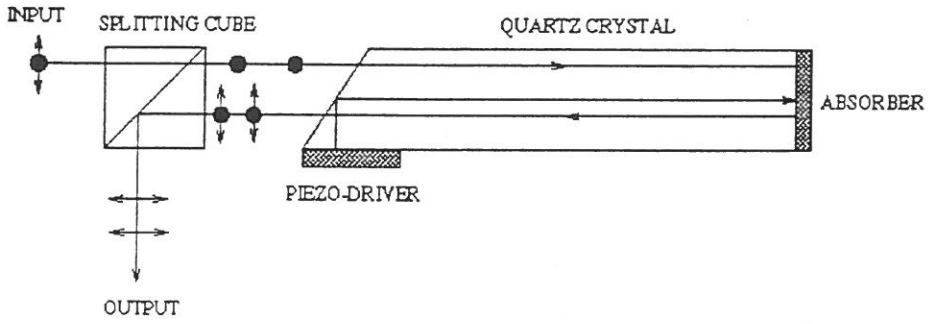

Figure 3.4 Optical diagram of the collinear quartz AOTF based on Anisotropic Bragg diffraction.

Figure 3.4 shows the optical layout of the AOTF crystal. The AOTF needed to be calibrated to determine the relationship between the control frequency and the wavelength. Ideally, this relation is given by a linear function,

$$f * \lambda = K * \Delta n \qquad (3.4)$$

where f is the frequency in MHz, λ is the wavelength of the transmitted wave, K is a constant and Δn is the difference of the refractive indices of the ordinary and extraordinary rays for crystalline quartz, which is the birefringence.

The AOTF was calibrated for the wavelength-control frequency relationship using different laser sources and narrow band pass filters. The data points are shown in Figure 3.2. The function is non-linear and a curve was fitted to the points to best fit the relation. A third degree polynomial was obtained which is given by,

$$f = (-1.4772e-6)\lambda^3 + 0.0028\lambda^2 - 1.9838\lambda + 570.7548 \qquad (3.5)$$

where f is the frequency in MHz and λ is the wavelength in nm.

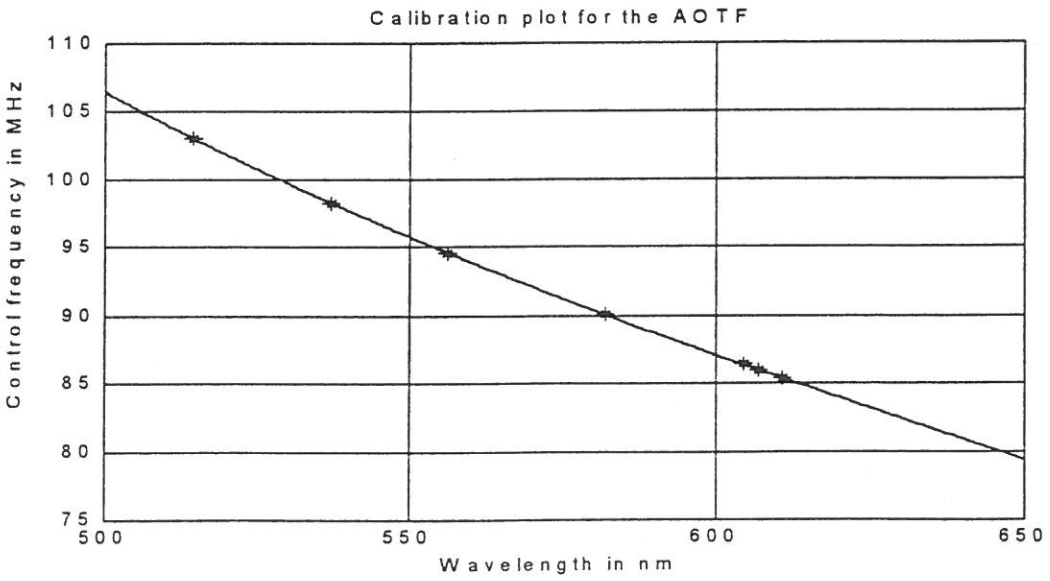

Figure 3.5. Calibration curve for the AOTF control frequency versus wavelength.

The deviation from the linear function can occur for many reasons. The primary reason could be attributed to the acoustic nonlinearities and/or multiple linear acousto-optic diffraction. The change in birefringence of the crystal as a function of wavelength also plays a role in the deviation from linearity. The acoustic nonlinearities occur mainly as a result of crystal lattice anharmonicities which distort the acoustic signal. Thus, an initially sinusoidal signal becomes distorted as it propagates and becomes a source of harmonic generation. In general, the nth harmonic grows non-linearly, at some distance it reaches a maximum, and then it decays. The exact form of this behavior depends critically upon the initial level of the signal, the quality of the crystal, and the acoustic attenuation of the crystal. When only one sinusoidal wave is propagating, the harmonics are integral multiples of the fundamental frequency and harmonic effects can be limited to power loss from the fundamental by using only an octave bandwidth. But when two sinusoidal signals with frequencies f_1 and f_2 respectively are propagating within the crystal, then the individual harmonics superimpose to cause appreciable effects. These are known as the elastic two-tone third-order intermodulation products (IMPs) and appear at frequencies $2f_1 - f_2$ and $2f_2 - f_1$.

Light diffracted from the first signal can be re-diffracted by the second signal and then re-diffracted by the first signal again. Both elastic

and dynamic IMPs represent unwanted spurious signals which degrade the spurious-free dynamic range of the AO device and hence needs careful analysis while designing high performance AO devices. These nonlinearities are discussed in detail by Goutzoulis [1994].

The AOTF driver circuitry generated the acoustic signal applied to the transducer attached to the face of the AOTF crystal. The high frequency acoustic wave and a modulating DC signal were applied to the driver circuitry. The modulation helps in keeping the average power of the signal applied to the AOTF within safe limits and provided better S/N ratio by permitting a background scan in the period when the modulation signal was low. The duty cycle of the modulation signal was approximately one-third, and the modulation cycle period was kept at 30 ms for the experiment which gave a reasonably good integration time for photon counting. The counter was programmed for an internal delay to take into account the delay time needed for the AOTF modulation and the propagation of the acoustic signal.

The AOTF is very sensitive to the degree of polarization of the incident light and it was found that unpolarized light increased the level of background signal. A polarizer was used in front of the input window to reduce the background and cut-off filter was used to filter out the green laser line.

3.3.3 Experimental Results

The results obtained from the experiments have been summarized in various plots and compared to the spectra obtained by B. Schrader [1989] which were published in his compilation titled "Raman/Infrared Atlas of Organic Compounds". Many common organic compounds were selected and the Raman spectrum studied using the AOTF. One of the samples was Ethylene Glycol which has the molecular formula $HO\text{-}CH_2\text{-}CH_2\text{-}OH$. The measured spectrum obtained is shown in Figure 3.6(a).

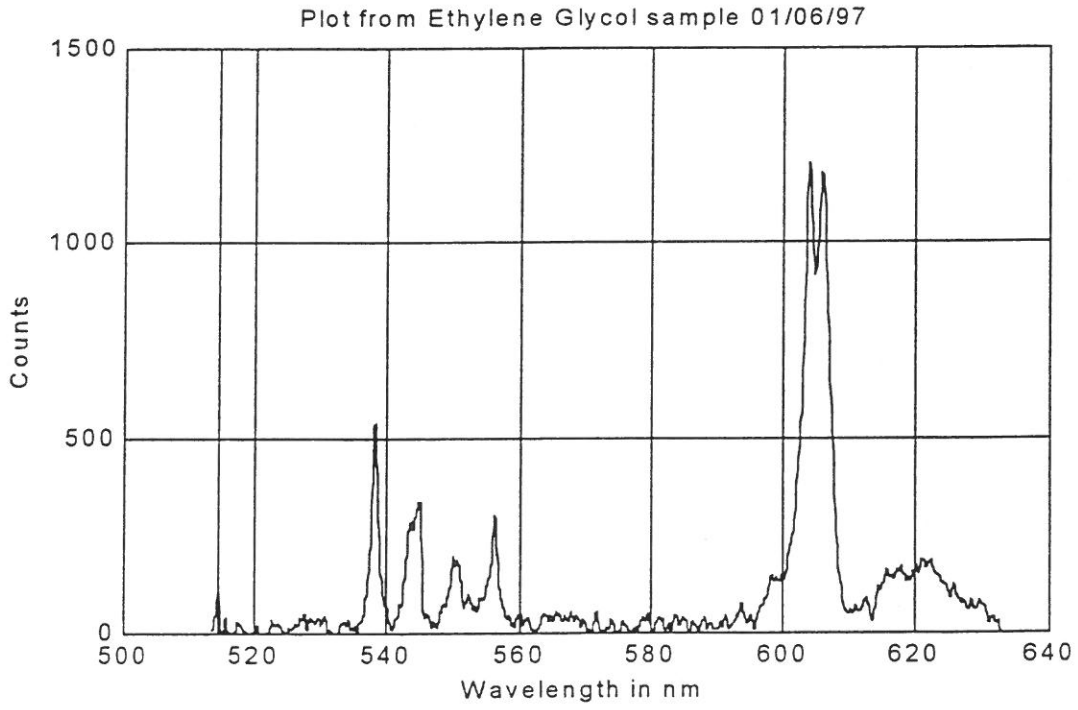

Figure 3.6 a. Intensity-Wavelength plot of Ethylene Glycol using the AOTF

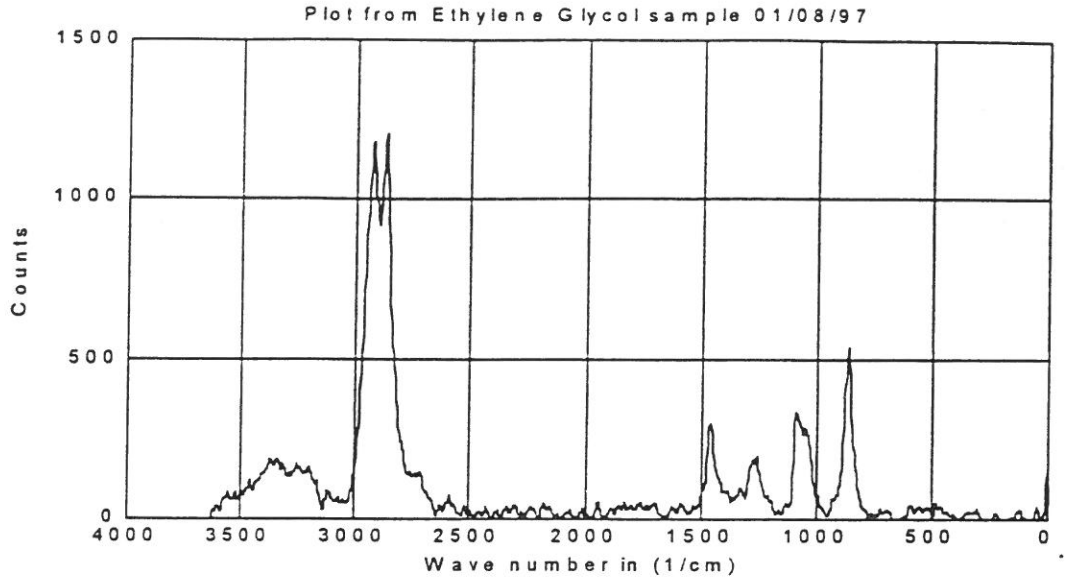

Figure 3.6 b. Raman spectra from Ethylene Glycol sample using the AOTF

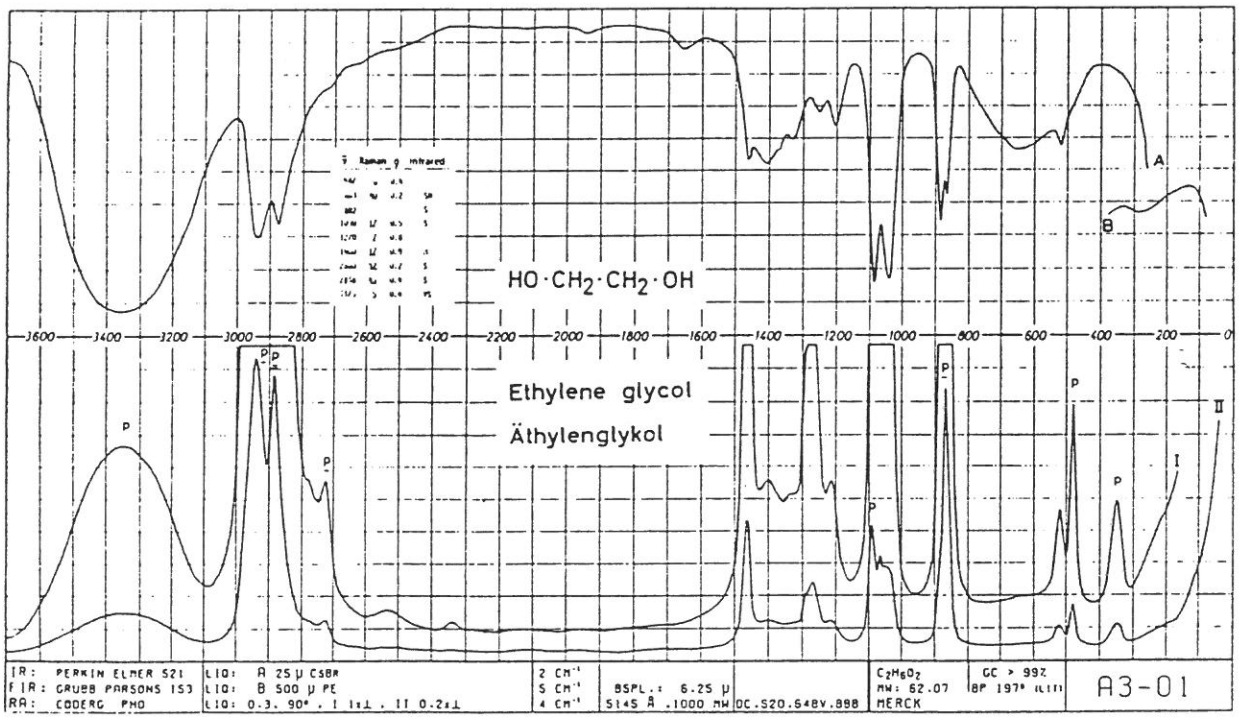

Figure 3.6 c. Spectra from Ethylene Glycol sample [Schrader, 1989]

The same spectrum converted from a wavelength scale to a wavenumber scale is shown in Figure 3.6(b) so that this spectrum could be compared to the spectrum obtained by Schrader which is shown in Figure 3.6 (c). The Raman spectra of Ethylene Glycol shown in Figure 3.6 (a) and (b) was obtained with the control frequency stepped in increments of 0.02 MHz for the scan, which corresponds to a spectral bandwidth of 3.5 cm^{-1} in wavenumber scale. Schrader had used a resolution between 2 cm^{-1} and 12 cm^{-1} depending on the properties of the substance scanned but 2 cm^{-1} was the spectral bandwidth generally used. There was no specific reason for choosing a stepping rate of 0.02 MHz. The data analysis was done in MATLAB where suitable filtering was done and background was subtracted to improve the S/N ratio. The MATLAB files used for the data processing are provided in Appendix A. Vibrational spectra was obtained for samples like methanol, chlorobenzene, liquid water, toluene, isopropanol, acetone, acetonitrile and a few others. Some of the spectra obtained are shown in the following figures and the remaining are given in Appendix B. The spectra obtained by Schrader is also shown for comparison.

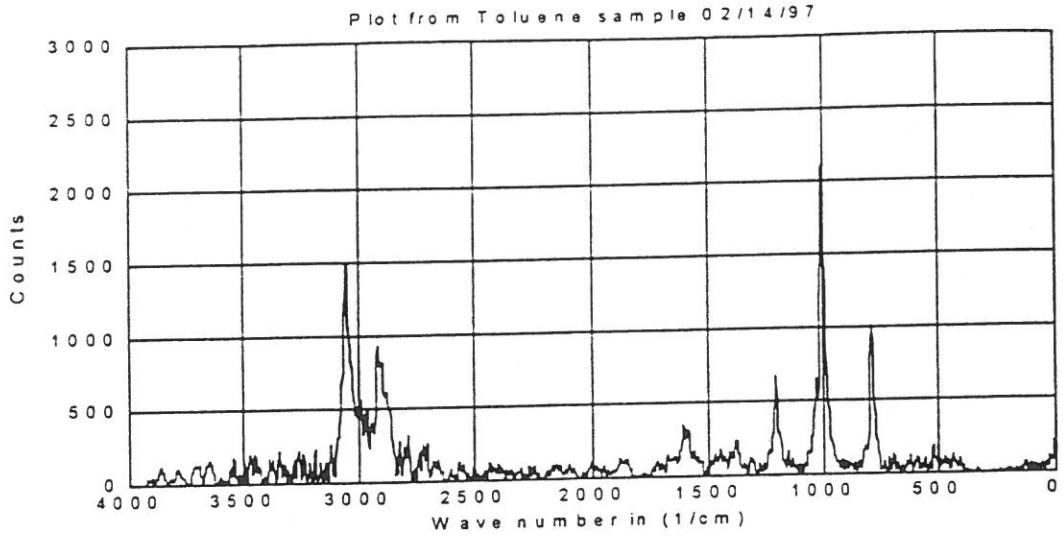

Figure 3.7 a. Raman spectra from Toluene sample using the AOTF

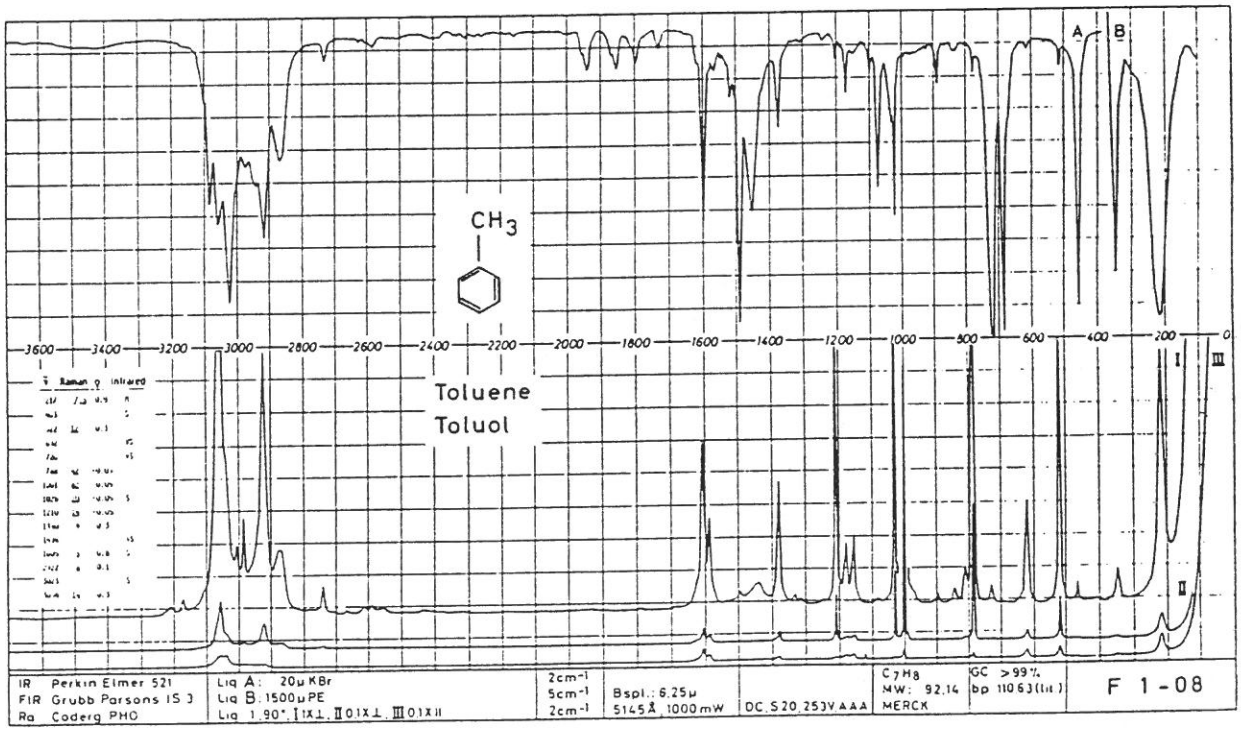

Figure 3.7 b. Spectra from Toluene sample [Schrader, 1989]

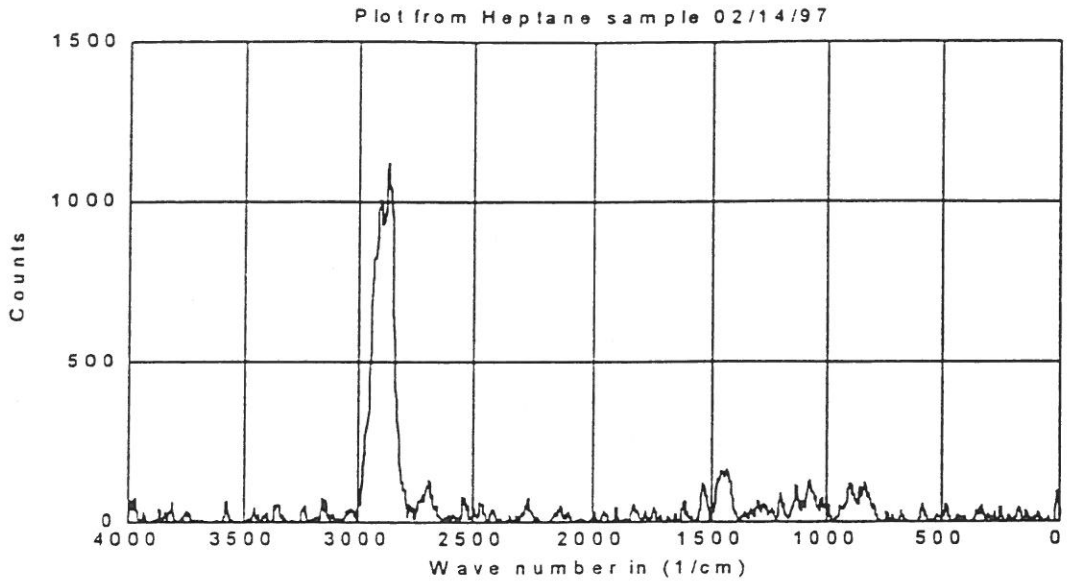

Figure 3.8 a. Raman spectra from Heptane sample using the AOTF.

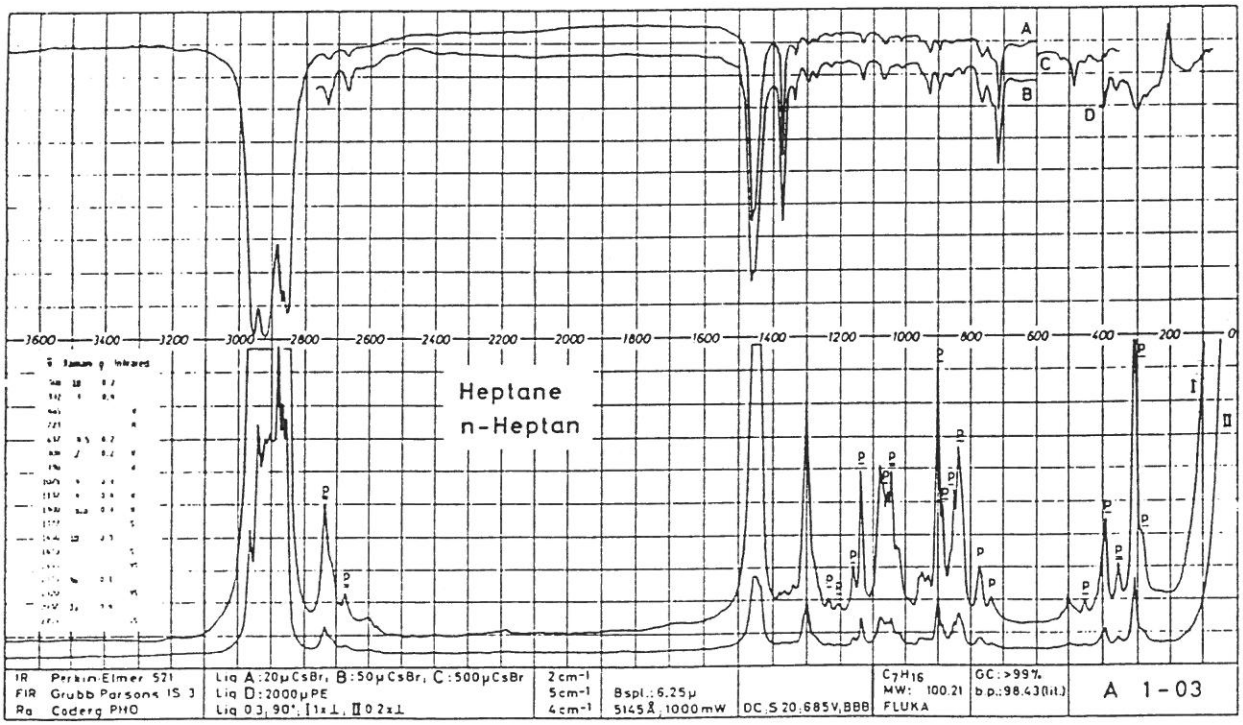

Figure 3.8 b. Spectra from Heptane sample [Schrader, 1989]

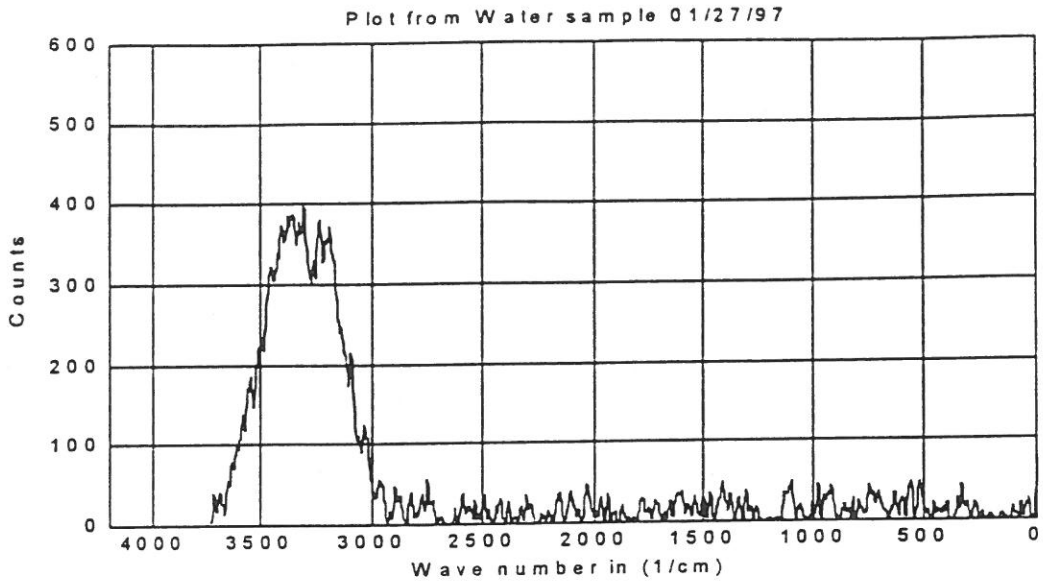

Figure 3.9 a. Raman spectra from de-ionized water sample using the AOTF.

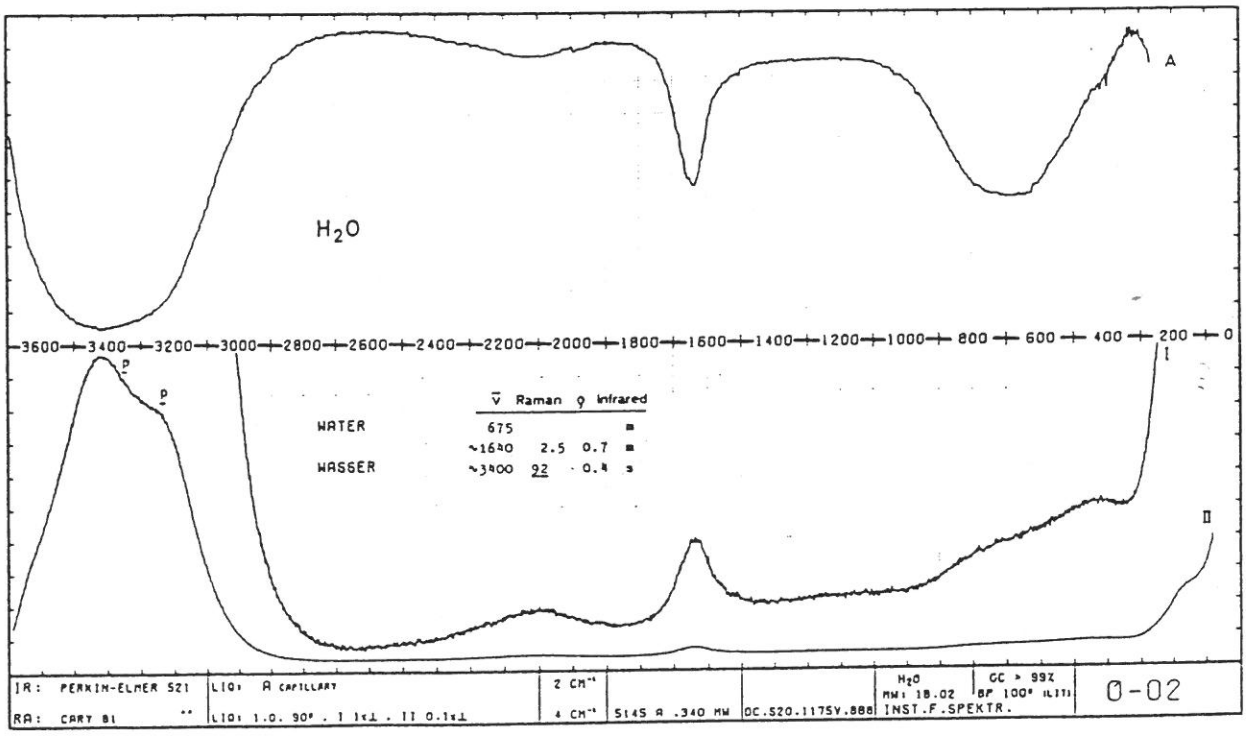

Figure 3.9 b. Spectra from Water sample [Schrader, 1989]

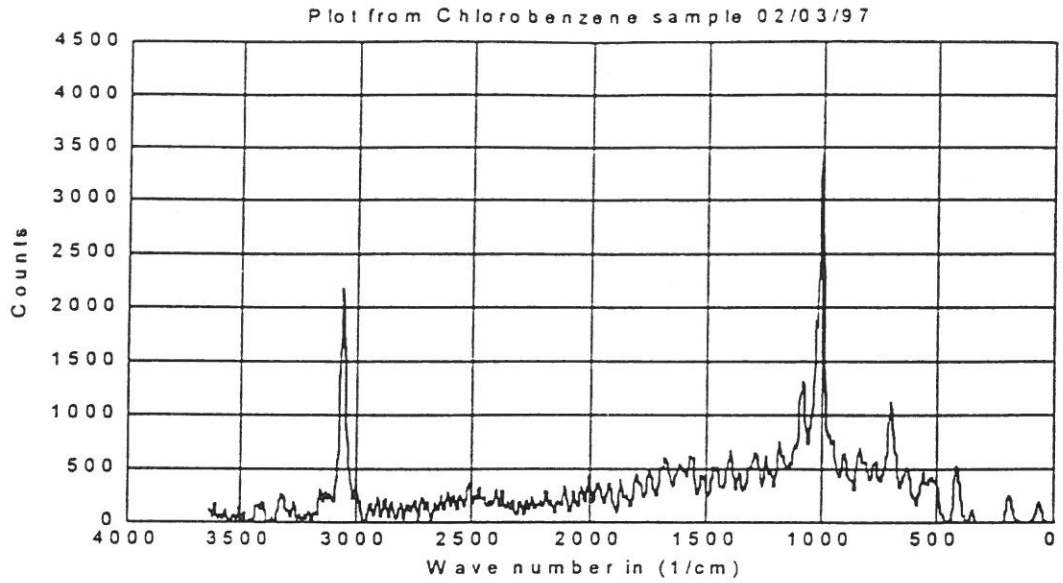

Figure 3.10 a. Raman spectra from Chlorobenzene sample using the AOTF

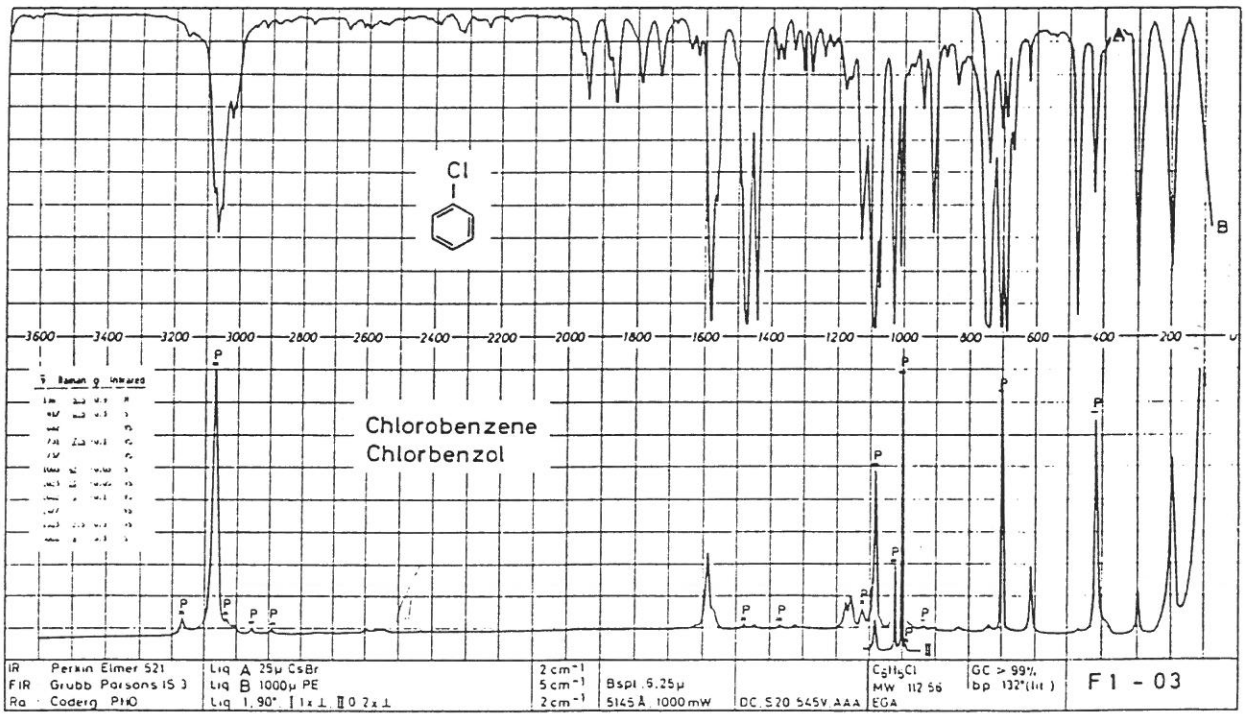

Figure 3.10 b. Spectra from Chlorobenzene sample[Schrader, 1989]

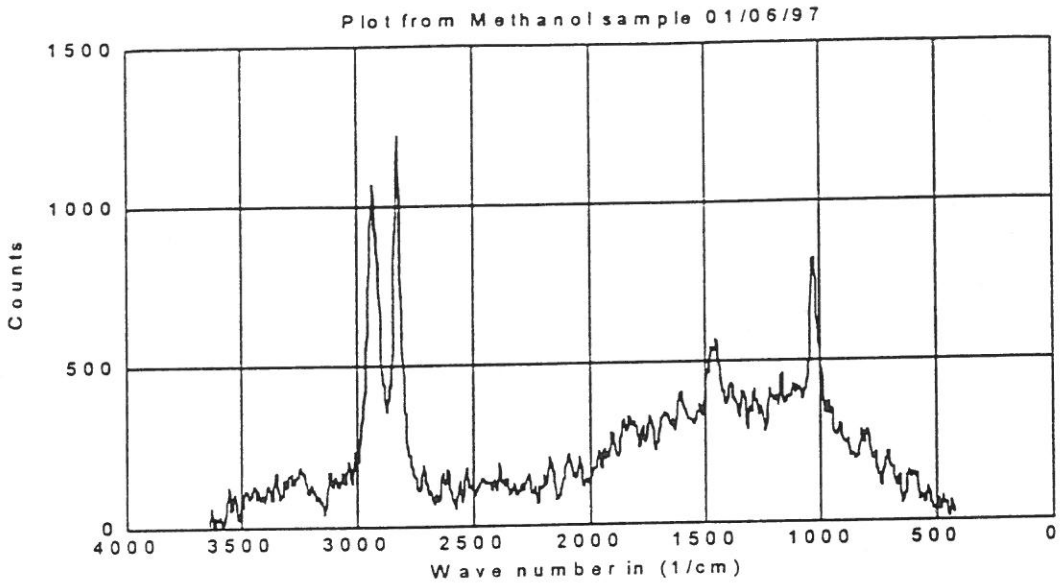

Figure 3.11 a. Raman spectra from Methanol sample using the AOTF

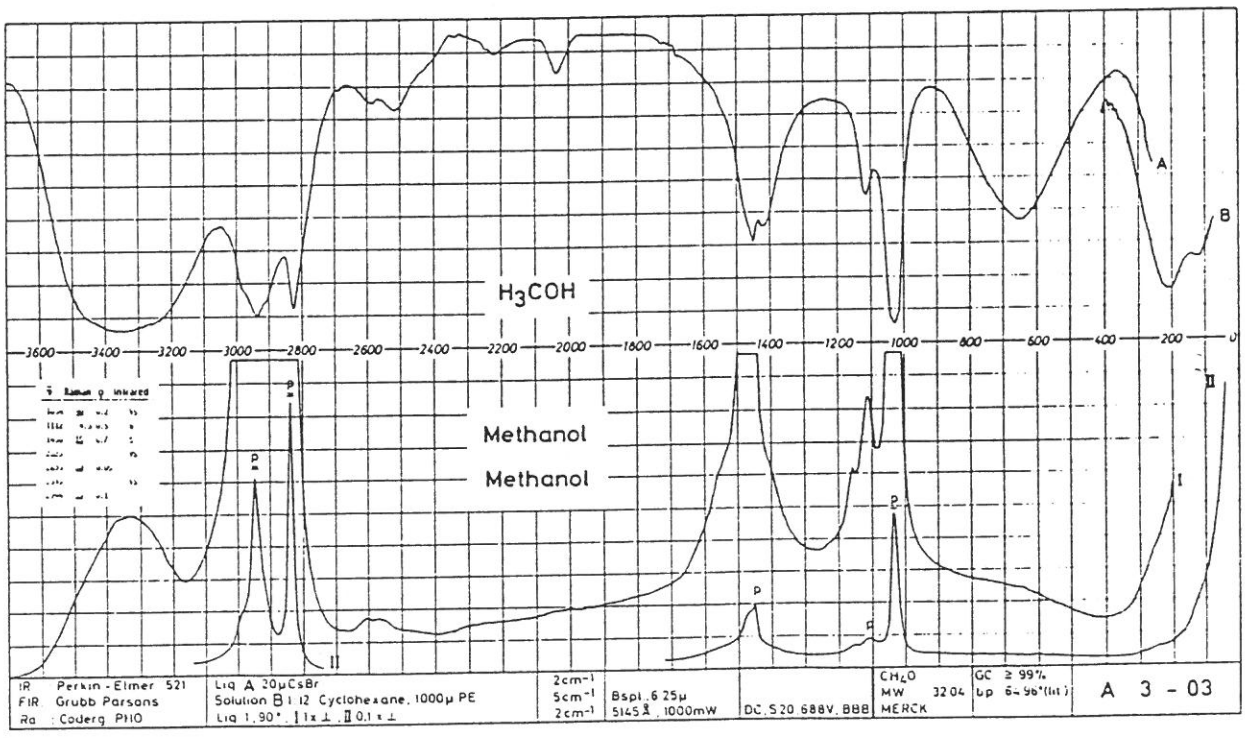

Figure 3.11 b. Spectra from Methanol sample [Schrader, 1989]

3.4 Experimental Inferences

The experiments which have been carried out provide validation for the use of the AOTF for different spectroscopic applications. The characteristics of the spectra obtained depend on the chemical properties of the sample [Schrader, 1995].

Table 3.2 Comparison of selected data points using the AOTF with those observed by Schrader.

Data points using the AOTF (cm^{-1})	Data points observed by Schrader (cm^{-1})
Ethylene Glycol:	
863.2	863
1461.2	1460
2875.9	2880
2931.3	2938
Isopropanol:	
815.1	819
2879.3	2882
2872.7	2975
2920.8	2920
Toluene:	
783.8	788
1001.8	1001
1029.5	1028
1210.3	1210
2920.9	2922
3055.8	3054
Acetonitrile:	
2934.8	2943
2252.1	2253
1380.8	1372

The data obtained by using the AOTF were compared to some of the data points obtained by Schrader's experiments [Schrader, 1989]. The relative intensities could not be compared as enough data was not available. But the wavenumbers could be compared quite accurately. Table 3.2 shows some of the values obtained using the AOTF and those observed by Schrader. The rms error in the wavenumber assignment for the data set was calculated to be 1.62%, assuming no error in the data points observed by Schrader.

3.5 Integration to the LIDAR system

The capabilities of the AOTF were successfully demonstrated in the laboratory. Our plan is to use it as an efficient detector unit in the LAMP lidar system. Several changes are needed to switch from a CW laser to a pulsed laser system due to timing and synchronization requirements. The signal intensities are also considerably lower and the signal light is transmitted through a optic-fiber. Since, the AOTF has a narrow incident angular aperture, an aspheric collimation package was used to collimate light at the end of the fiber. Other parts were machined so that additional optics, filters and polarizers, could be added at the input of the AOTF. A Hamamatsu PMT was used for photon collection and photon counting was accomplished using the SR 430 unit.

3.5.1 The LAMP lidar instrument

The LAMP lidar which was developed at Penn State University and improved over the past several years has focused on the application of Raman vibrational and rotational scattering techniques [Philbrick, 1994]. Measurements have been carried out during several campaign periods which demonstrate the performance of Raman lidar techniques compared to standard meteorological rawinsonde balloon payload measurements [Harris et al., 1996]. The LAMP lidar consists of five primary subsystems: transmitter, receiver, detector, data system, and safety system [Stevens, 1992]. The transmitter is a Nd:YAG laser with output wavelengths at 532 nm and either 355 or 266 nm. The laser operates at a pulse repetition rate of 20 Hz, emitting 7 nsec pulses with energies of 400 mJ, 250 mJ, and 85 mJ, at the respective wavelengths. The laser pulses are directed into the atmosphere off of three hard coated mirrors in a monostatic arrangement relative to the receiver. The backscattered light signal is directed from an optical flat into a 16" classical Cassigrain telescope which is coupled to a one millimeter diameter optical fiber that directs the signal into the detector. Detector units which emphasize high altitude (5 to 80 km) and low altitude (surface to 10 km) measurements have been prepared. This effort is concerned with the detector unit that was designed primarily for low altitude measurements. It incorporates the vibrational Raman

measurements of water vapor and optical extinction with rotational Raman temperature measurement capabilities.

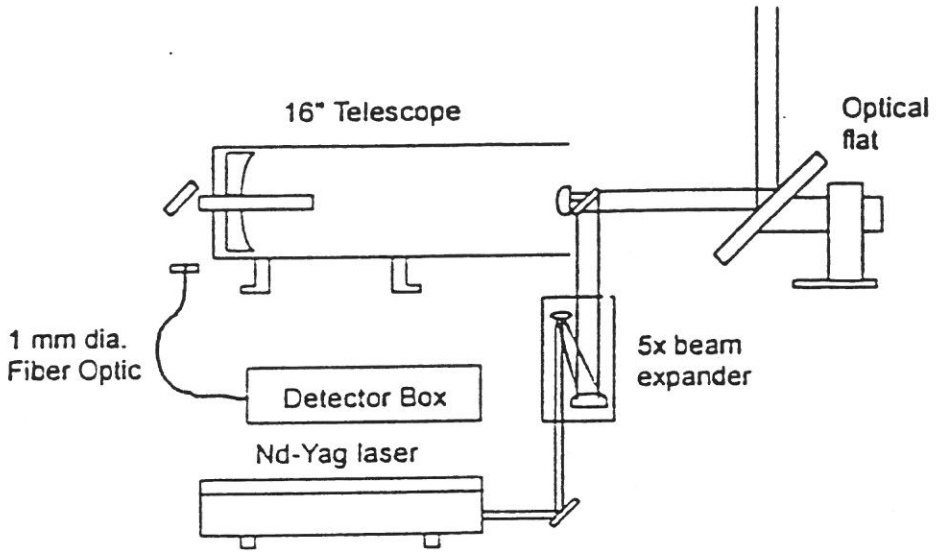

Figure 3.12. Schematic diagram of the Penn State LAMP lidar [Haris, 1995].

The lidar configuration is shown in Figure 3.10. The detector box measures signals derived from the 532 nm wavelength and uses ultraviolet signals derived from either the 355 or 266 nm wavelengths. The scattering from the 532 nm laser beam provide information on temperature, water vapor concentration, nitrogen concentration, molecular density, and aerosol extinction. The signal derived from the 355 nm can be used to provide the same information. When the 266 nm crystal is installed in the

laser, then profiles of ozone density, and the water vapor concentration can be obtained during daytime using the "solar blind" region of the spectrum.

Signals from the 266 nm wavelength can even be measured during the day because they are in the "solar blind" region which occurs due to stratospheric ozone shielding of the solar ultraviolet wavelengths. The detection system used today is typically comprised of a series of beam splitters coupled with narrow band filters centered at wavelengths of interest with photomultiplier tubes for each wavelength channel.

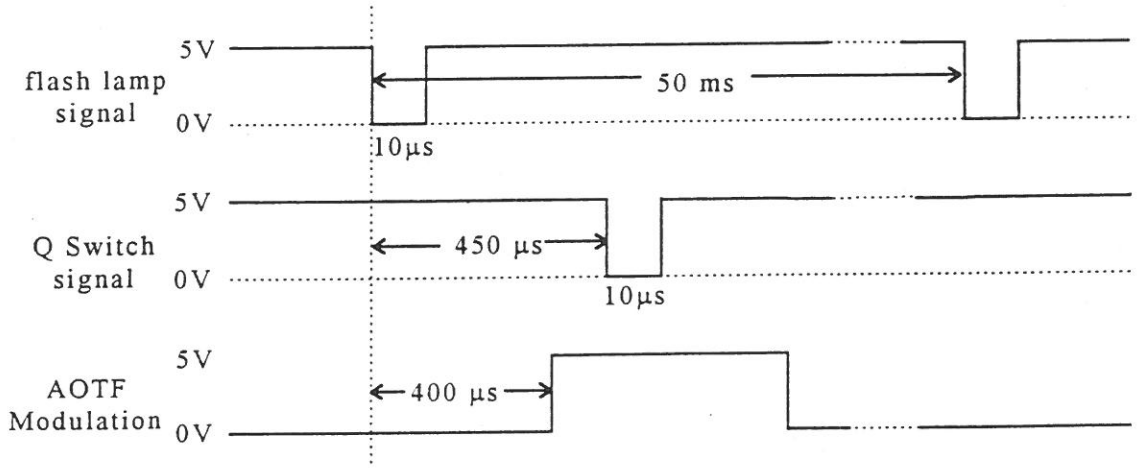

Figure 3.13. Timing diagram for AOTF modulation and laser signals.

The two important signals provided by laser are the initiation of the flash lamp and the Q switch. The timing diagram is illustrated in Figure 3.11. The flash lamp signal is a 10 μs wide negative going pulse which had a frequency of 20 Hz. The Q switch signal was similar to the flash lamp signal but occurred about 450 μs after the flash lamp signal and initiates

the laser pulse. The AOTF modulation was synchronized to occur 50 μs before the Q switch and hence gave ample time for the phase grating to set up within the AOTF crystal. The counting was synchronized to the Q switch signal and internal bin widths were selected in the SR 430 to give an altitude resolution of 80 m. The integration time for each control frequency was set for 1 minute.

The settings for the function generator and the photon counter were accomplished using a QBASIC source code (a copy is presented in Appendix C). The experimental attempt was to determine some of the prominent constituents in the atmosphere like nitrogen, oxygen and water vapor. These efforts are still continuing and a lot of optimism exists in getting useful results.

Chapter 4

CONCLUSIONS

An examination into the use of an Acousto-Optic Tunable Filter (AOTF) for spectroscopy has been made. The versatility of the AOTF and its ability to show accurate Raman scattering profiles of various species have been effectively demonstrated. This research attempts to highlight the advantages of the AOTF and the feasibility of its use in many other applications.

4.1 Future work

The AOTF is currently being integrated to the LAMP lidar system. The success of this effort should lead to the AOTF being used for detection of pollution species from smoke stack emissions. In achieving this objective, it would be practical to incorporate the LARS lidar system in which the laser is mounted on a scanning platform. The system houses a Continuum Surelight II-20 laser on a platform which has a scanning range of 60° from the azimuth. Figure 4.1 illustrates the proposed use of this system for detection of species from smoke stacks. A list of possible species which can be detected by the system is also shown in the figure.

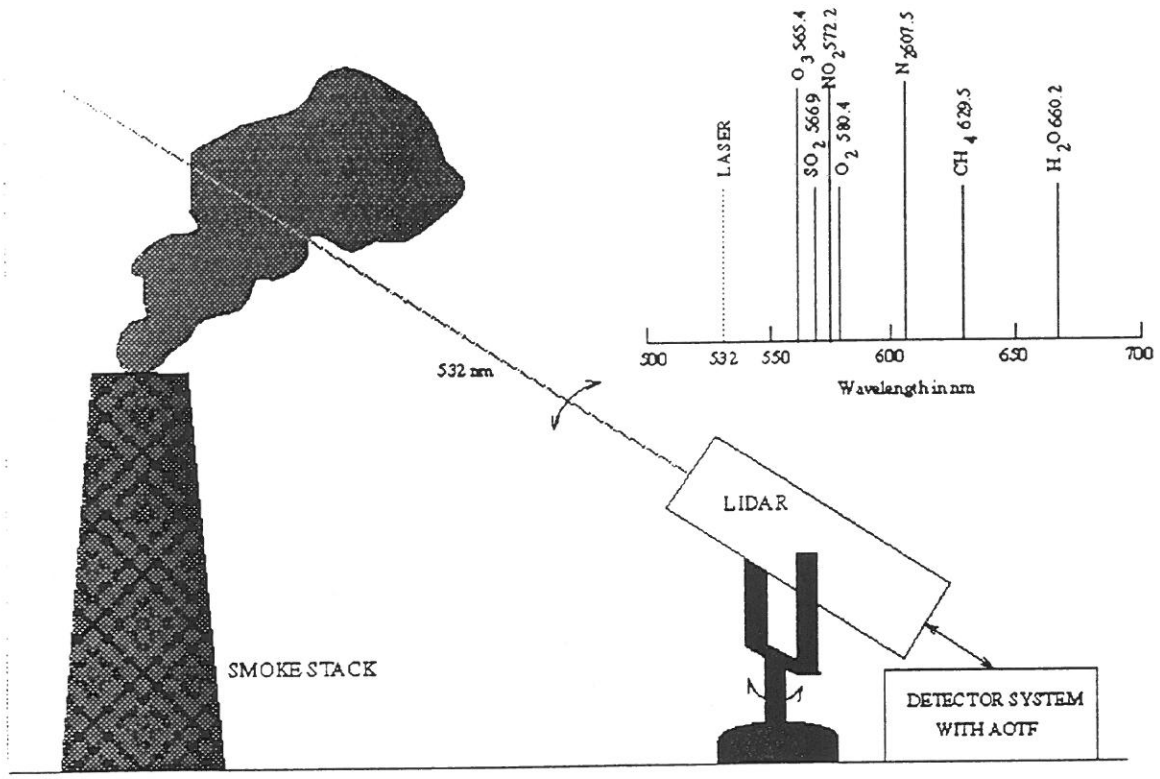

Figure 4.1 A scanning lidar using an AOTF for detection of species in smoke stacks.

There are many more exciting research areas where the use of an AOTF can be justified. AOTFs designed to operate in the UV spectral range have been produced and this can be effectively used for real time monitoring of important pollution species. Ozone, NO_2, and SO_2 can be effectively monitored using an UV source and AOTF as a detection system. AOTFs are also being used in spectral imaging, bio-medical and chemical applications.

REFERENCES

Chang, I.C., "Acousto-optic devices and applications," IEEE Transactions on Sonics Ultrasonics, Vol. 23, 2-22 (1976).

Dixon, R.W., "Acoustic diffraction of light in anisotropic media," IEEE Journal of Quantum Electronics, Vol. QE-3, No.2, 85-93 (1967).

Goutzoulis, A.P., Pape, D.R., *Design and fabrication of acousto-optic devices*, New York: Marcel Dekker Inc. (1994).

Haris, P.A.T, "Pure rotational Raman lidar for temperature measurements in the lower troposphere," Ph.D Thesis, The Pennsylvania State University (1995).

Harris, S.E., Wallace, R.W., "Acousto-optic tunable filter," Journal of the Optical Society of America, Vol. 59, No.6 744-747 (1969).

Herzberg, G., *Molecular spectra and molecular structure :I. spectra of diatomic molecules*, Florida: Robert E. Krieger Publishing (1989).

Klein, W.R., Cook, B.D, "Unified approach to ultrasonic light diffraction," IEEE Transactions on Sonics-Utrasonics, Vol. 14, 123-134 (1967).

Kogelnik, H., "Coupled wave theory for thich hologram gratings," Bell System Technical Journal, Vol. 48, 2909-2949 (1969).

Phariseau, P., "On the diffraction of light by progressive ultrasonic waves," Proceedings of the Indian Academy of Sciences, Vol. 44A, 165-170 (1956).

Philbrick, C.R., "Raman lidar measurements of atmospheric properties," Proceedings of Atmospheric Propagation and Remote Sensing III, SPIE 22222, 922-931 (1994).

Pustovoit, V.I., V.E.Pozhar, "Collinear diffraction of light by sound waves in crystals: devices, applications and new ideas," Photonics and Optoelectronics 2, 53-69 (1994).

Raman, C.V., Nath, N.S.N., "Diffraction of light by high frequency sound waves," Indian Academy of Sciences, Parts 1,2 (1935); Parts 3-5 (1936).

Schrader, B., *Infrared and Raman spectroscopy: methods and applications*, VCH Publishers Inc.(1995).

Schrader, B., "Raman/infrared atlas of organic compounds," Second edition, (1989).

Stevens, T.D., "An optical detection system for a Rayleigh/Raman lidar," MS Thesis, The Pennsylvania State University (1992).

Appendix A

DATA PROCESSING SOURCE CODES

This section contains the matlab source codes used for the data processing.

```
% This program plots the spectrum from any sample with wave number on the X
axis.
% This applies a hamming filter on the signal as well as the background and
then does the
%bgnd subtraction.

function meth(abc);
c =abc(:,3);
f= abc(:,2);
a = size(abc,1);
b = (a/2);

%loop to separate signal data into a column vector
j = 1;
i = 1;
while j<=b,
    c2(j) = c(i);
    f2(j) = f(i);
    j=j+1;
    i=i+2;
end
n=3;
while n<(b-1),
      x = [ c2(n-2)  c2(n-1)  c2(n)  c2(n+1)  c2(n+2)]* hamming(5);
      c2(n)=x;
      n = n+1;
end

%loop to separate the background data into a column data
j = 1;
i = 2;
while j<=b,
    c3(j) = c(i);
    f3(j) = f(i);
    j=j+1;
    i=i+2;
end
n=3;
while n<(b-1),
```

```
      x = [ c3(n-2)  c3(n-1)  c3(n)  c3(n+1)  c3(n+2)]* hamming(5);
      c3(n)=x;
      n = n+1;
end

% this part subtracts the background from the signal
j = 1;
while j<=b,
      c4(j) = c2(j) - c3(j);
      if c4(j)<0
            c4(j)=0;
      end
      j=j+1;
end

%this part smooths the data using a hamming filter
n=3;
j=1;
while n<(b-1),
      x = [ c4(n-2)  c4(n-1)  c4(n)  c4(n+1)  c4(n+2)]* hamming(5);
      c5(n)=x;
      fn(j)=f2(n);
      cn(j)=c5(n);
      n = n+1;
      j = j+1;
    end

% m file to calculate the calibration curve for the AOTF

lamda = [514.5 537.1 556.3 581.9 604.7 606.3 607.2 610.9];
freq = [103.12 98.3 94.6 90.08 86.36 86.13 85.94 85.4];
[p,s] = polyfit(freq,lamda,3);
w = ((fn.^3)*p(1) + (fn.^2)*p(2) + fn*p(3) + p(4));
z = 1./w;
whitebg;
plot(-(((1/514.5)-z)*1e7),cn,'b');
grid;
axis([-4000 0 0 1500]);
temp = get(gca,'xticklabel')
xtemp = (-1).*(str2num(temp))
set(gca,'xticklabel',[xtemp]);
title('Plot from Water sample 01/27/97');
xlabel('Wave number in (1/cm)');
ylabel ('Counts');


% This program plots the spectrum from any sample with wavelength on the X
axis.
% This applies a hamming filter on the signal as well as the background and
then does the
%bgnd subtraction.


function acet2(abc);
```

```
c =abc(:,3);
f= abc(:,2);
a = size(abc,1);
b = (a/2)
%loop to separate signal data into a column vector
j = 1;
i = 1;
while j<=b,
    c2(j) = c(i);
    f2(j) = f(i);
    j=j+1;
    i=i+2;
end

n=3;
while n<(b-1),
      x = [ c2(n-2) c2(n-1) c2(n) c2(n+1) c2(n+2)]* hamming(5);
      c2(n)=x;
      n = n+1;
end

%loop to separate the background data into a column data
j = 1;
i = 2;
while j<=b,
    c3(j) = c(i);
    f3(j) = f(i);
    j=j+1;
    i=i+2;
end
n=3;

while n<(b-1),
      x = [ c3(n-2) c3(n-1) c3(n) c3(n+1) c3(n+2)]* hamming(5);
      c3(n)=x;
      n = n+1;
end

% this part subtracts the background from the signal
j = 1;
while j<=b,
      c4(j) = c2(j) - c3(j);
      if c4(j)<0
            c4(j)=0;
      end
      j=j+1;
end

%this part smooths the data using a hamming filter
n=3;
j=1;
while n<(b-1),
      x = [ c4(n-2) c4(n-1) c4(n) c4(n+1) c4(n+2)]* hamming(5);
```

```
        c5(n)=x;
        fn(j)=f2(n);
        cn(j)=c5(n);
        n = n+1;
        j = j+1;
end
t = size(fn);
% m file to calculate the calibration curve for the AOTF
lamda = [514.5 537.1 556.3 581.9 604.7 606.3 607.2 610.9];
freq = [103.12 98.3 94.6 90.08 86.36 86.13 85.94 85.4];
[p,s] = polyfit(freq,lamda,3);
w = ((fn.^3)*p(1) + (fn.^2)*p(2) + fn*p(3) + p(4));
h = size(w);
whitebg;
plot(w,cn,'b');
grid
hold on
plot([514.5 514.5], [0 700], 'g');
title('Plot from Water sample 01/27/97');
xlabel('Wavelength in nm');
ylabel ('Counts');


% m file to deteremine the rms error fo data.

X= [2931.32 2875.89 863.2 1461.17 2934.8 2252.12 1380.85 2917.4 2920.8
2972.8 2979.3 815 3055.8 2920.9 1210.3 1029.6 1001.8 783.8]
Y= [2938 2880 863 1460 2943 2253 1372 2925 2920 2975 2882 819 3054 2922
1210 1028 1001 788]
n = size(X)
k = size(Y)
h = n-1;
total =0;
for i = 1:n,
  total = total + ((X(i)-Y(i))^2)
end
err = (((total ./h(2)))^0.5)
plot (X,Y);
```

Appendix B

EXPERIMENTAL RESULTS

This section contains the Raman spectra of organic samples not included in Chapter 3.

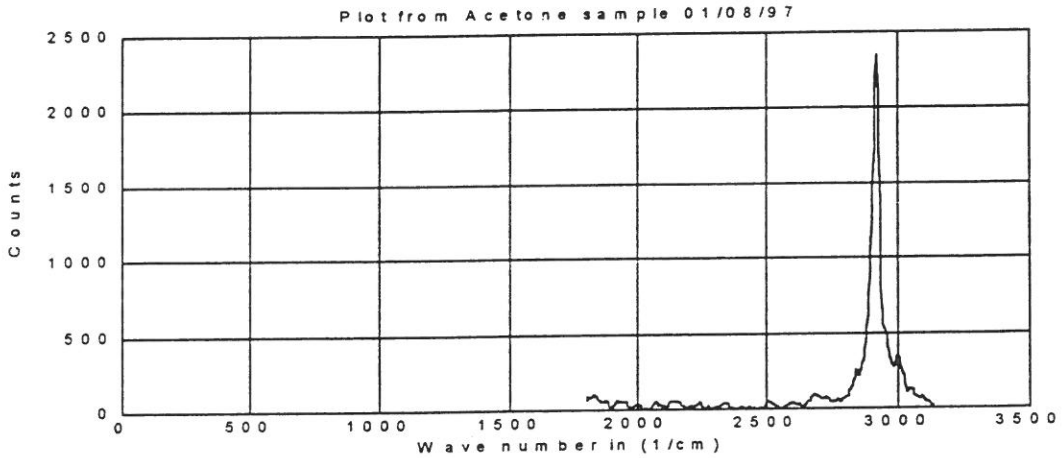

Spectra from acetone sample

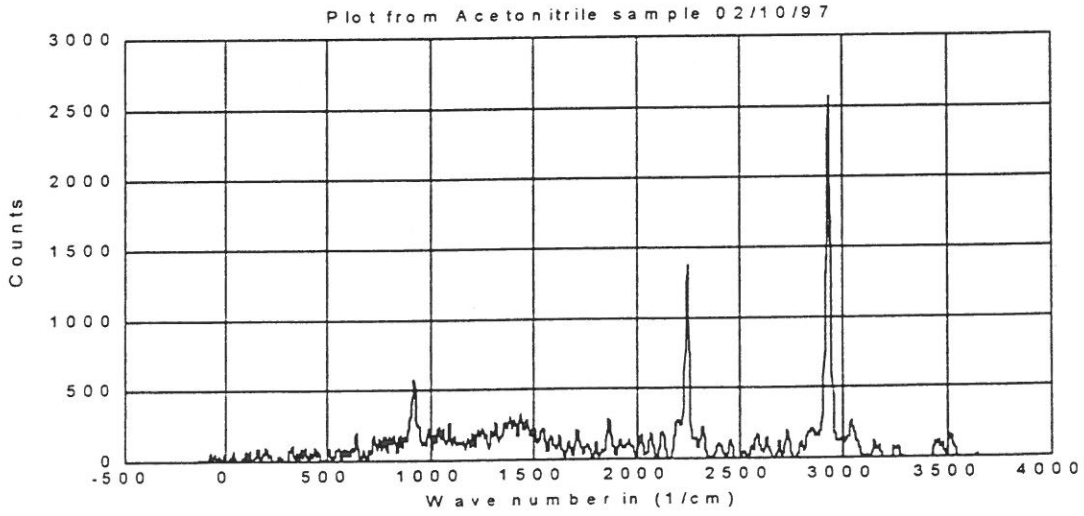

Spectra from Acetonitrile sample.

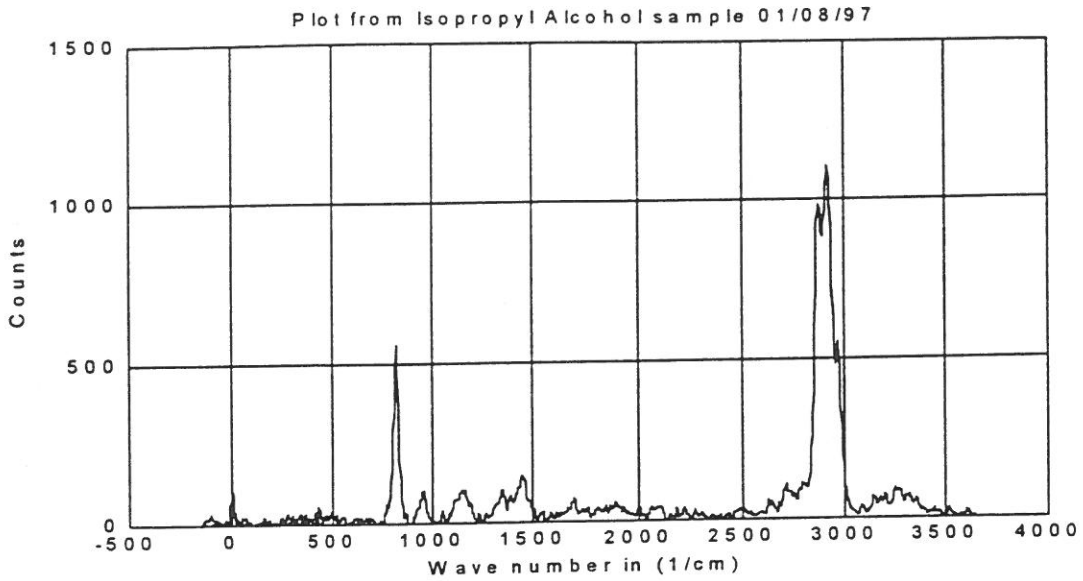

Spectra from isopropanol sample

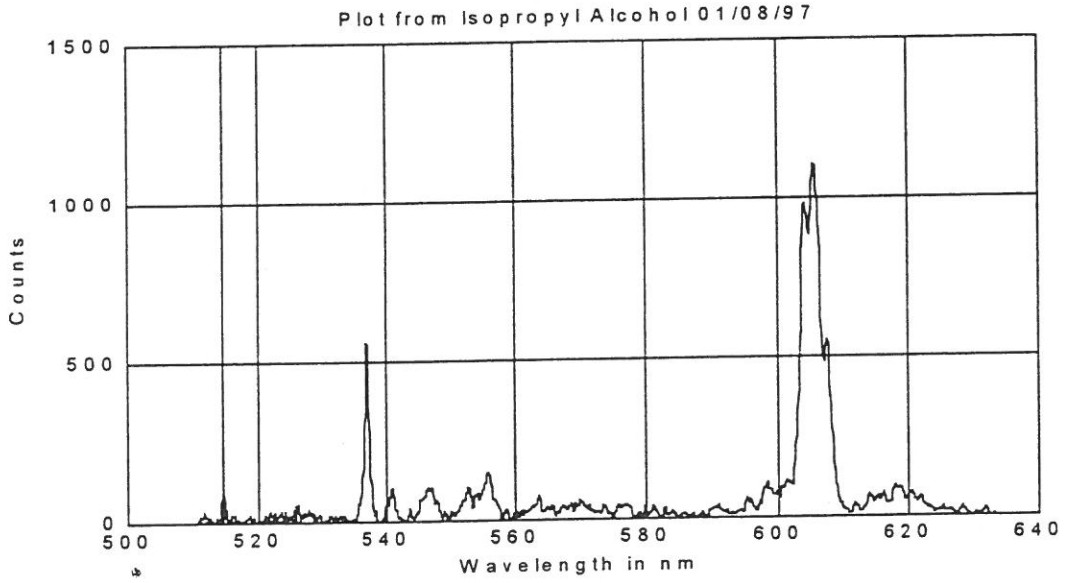

Spectra from isopropanol sample on wavelength scale.

Appendix C

COMPUTER INTERFACE SOURCE CODES

This section contains the QBASIC source codes used for the hardware interface and data acquisition.

```
' Program to use SRS multichannel scaler/averager  SR430
' for measuring  counts with a constant
' discriminator level
' for determining a spectrum of a particular sample using the AOTF
' Configure the SRS430 to 19.2 kbaud, 8 bits, no parity before running the
' program. Use RS232 connection on com1.
'The HP function generator is controlled by the GPIB interface

CLS
'This part of the program controls the HP8656A instrument via GPIB.
'The instrument address is 19. The base address of the card is set to
'&HD000. The I/O address is &H2B8.

CLS
DEF SEG = &HD000

'Reset the GPIB card
init% = 0
ioport% = &H2B8
myaddr% = 21
setting% = &H100
PRINT "Reset Card..."
CALL absolute(ioport%, myaddr%, setting%, init%)

'Code to output command string to device
offset% = 3
addr% = 19          ' address of HP8656A instrument

'Turn AM off
d$ = "AMS4"
PRINT USING "Device = ###, Command = \                    \"; addr%; d$
CALL absolute(addr%, d$, offset%)

'Set Amplitude
d$ = "AP1000MV"
PRINT USING "Device = ###, Command = \                    \"; addr%; d$
CALL absolute(addr%, d$, offset%)
```

```
'Preset Frequency
d$ = "FR100MZ"
PRINT USING "Device = ###, Command = \                    \"; addr%; d$
CALL absolute(addr%, d$, offset%)

start:
CLS
  INPUT "Enter today's date: ", dat$
t$ = "d:\AOTFDATA\" + LTRIM$(dat$)
g$ = "d:\TOM\param.dat"
OPEN g$ FOR OUTPUT AS #5

INPUT "Enter the name of the file to store the data: ", file$
f$ = "d:\AOTFDATA\" + LTRIM$(dat$) + "\" + LTRIM$(file$)

INPUT "Enter the starting frequency (in MHz): ", fstart!
INPUT "Enter the ending frquency (in MHz): ", fend!
INPUT "Enter the increment for each step (in MHz): ", incr!
INPUT "Are you sure all the data entered is correct (y/n) :", ans$


IF LCASE$(ans$) = "n" THEN
     GOTO start
ELSE
END IF


ON ERROR GOTO newdir
MKDIR t$
newdir:


OPEN f$ FOR OUTPUT AS #1   ' FILENAME
PRINT "The file opened is : ", f$

WRITE #5, file$, fstart!, fend!, incr!
CLOSE #5
' PARAMETERS TO SET BEFORE RUNNING

OPEN "COM1:9600,N,8,2,CS,DS,CD" FOR RANDOM AS #2
TALK$ = "OUTP 0"    'DIRECT SR430 OUTPUT TO RS232 PORT
PRINT #2, TALK$
TALK$ = "BWTH 9"   'SET BINWIDTH TO 10.24 uS
PRINT #2, TALK$
TALK$ = "BREC 1"    'SET RECORD LENGTH TO 1024 BINS
PRINT #2, TALK$
TALK$ = "RSCN 1"    'SET SCAN PER RECORD 1
PRINT #2, TALK$
TALK$ = "TRLV 1.0"   'SET TRIGGER LEVEL TO +1.0V
PRINT #2, TALK$
TALK$ = "TRSL 0"    'SET TRIGGER SLOPE TO POSITVE
PRINT #2, TALK$
TALK$ = "DCSL 1"    'SET DISCRIMINATOR SLOPE TO NEGATIV
PRINT #2, TALK$
```

```
PRINT #2, "DCLV -10E-3"       'SET DISCRIMINATOR"
PRINT #2, "DCLV?"       'QUERY DISCRIMINATOR
INPUT #2, discr!
PRINT "The discriminator is set to:", discr!, "Volts"

k = fstart!
i = 0
WHILE k! <= fend!
 i = i + 1
 freq = k!
 d$ = "FR" + LTRIM$(STR$(freq)) + "MZ"
 'PRINT USING "Device = ###, Command = \                    \"; addr%; d$
 CALL absolute(addr%, d$, offset%)
 k! = k! + incr!

     PRINT #2, "CLRS"
     TALK$ = "TRSL 0"     'SET TRIGGER SLOPE TO POSITVE
     PRINT #2, TALK$
     PRINT #2, "BOFF 16"  'set trigger offset to 16*bin width
     PRINT #2, "SSCN"
     scannum = 0
     WHILE scannum <> 1
     PRINT #2, "SCAN?"
    INPUT #2, scannum
    WEND
    PRINT #2, "STAT"
    PRINT #2, "SPAR? 2"
   INPUT #2, count

 'Write i, mean to file and screen
 PRINT #1, i, freq, count
 PRINT i, freq, count

 'This part of the loop does a scan in the off period of modulated signal

 PRINT #2, "CLRS"
 TALK$ = "TRSL 1"     'SET TRIGGER SLOPE TO NEGATIVE
 PRINT #2, TALK$
 PRINT #2, "BOFF 480"  'set trigger offset to 480*bin width


 PRINT #2, "SSCN"
 scannum = 0
 WHILE scannum <> 1
  PRINT #2, "SCAN?"
  INPUT #2, scannum
 WEND

 PRINT #2, "STAT"
 PRINT #2, "SPAR? 2"
 INPUT #2, count

 'Write i, mean to file and screen
```

```
  PRINT #1, i, freq, count
  PRINT i, freq, count
WEND

END
```

```
'THIS WORKS FOR A SINGLE CONTROL FREQUENCY.....


' Program to use SRS multichannel scaler/averager SR430
' for measuring  counts with a constant
' discriminator level
' for determining a spectrum of a particular sample using the AOTF
' Configure the SRS430 to 19.2 kbaud, 8 bits, no parity before running the
' program. Use RS232 conection on com1.
'The HP function generator is controlled by the GPIB interface

CLS
'This part of the program controls the HP8656A instrument via GPIB.
'The instrument address is 19. The base address of the card is set to
'&HD000. The I/O address is &H2B8.


DEF SEG = &HD000

'Reset the GPIB card
init% = 0
ioport% = &H2B8
myaddr% = 21
setting% = &H100
PRINT "Reset Card..."
CALL absolute(ioport%, myaddr%, setting%, init%)

'Code to output command string to device
offset% = 3
addr% = 19          ' address of HP8656A instrument

'Turn AM off
d$ = "AMS4"
PRINT USING "Device = ###, Command = \                    \"; addr%; d$
CALL absolute(addr%, d$, offset%)

'Set Amplitude
d$ = "AP1000MV"
PRINT USING "Device = ###, Command = \                    \"; addr%; d$
CALL absolute(addr%, d$, offset%)

'Preset Frequency
d$ = "FR100MZ"
PRINT USING "Device = ###, Command = \                    \"; addr%; d$
CALL absolute(addr%, d$, offset%)

start:
CLS
  INPUT "Enter today's date: ", dat$
INPUT "Enter the time for run (in minutes): ", inttime
INPUT "Enter the name of the directory to store the data: ", dir$
t$ = "d:\AOTFDATA\" + LTRIM$(dat$) + "\" + LTRIM$(dir$)
g$ = "d:\TOM\param.dat"
OPEN g$ FOR OUTPUT AS #5
```

```
INPUT "Enter the frequency (in MHz): ", fstart!

INPUT "Are you sure all the data entered is correct (y/n) :", ans$

IF LCASE$(ans$) = "n" THEN
      GOTO start
ELSE
END IF

ON ERROR GOTO newdir
MKDIR t$
newdir:

WRITE #5, file$, fstart!, fend!, incr!
CLOSE #5
' PARAMETERS TO SET BEFORE RUNNING

OPEN "COM1:9600,N,8,2,CS,DS,CD" FOR RANDOM AS #2
talk$ = "OUTP 0"    'DIRECT SR430 OUTPUT TO RS232 PORT
PRINT #2, talk$
talk$ = "BCLK 0"   'SET BINCLOCK TO INTERNAL
PRINT #2, talk$

talk$ = "BWTH 4"   'SET BINWIDTH TO 320 ns
PRINT #2, talk$
talk$ = "BREC 1"    'SET RECORD LENGTH TO 1024 BINS
PRINT #2, talk$
talk$ = "RSCN 1200"    'SET SCANS PER RECORD 1200
PRINT #2, talk$
talk$ = "TRLV 1.0"   'SET TRIGGER LEVEL TO +1.0V
PRINT #2, talk$
talk$ = "TRSL 0"    'SET TRIGGER SLOPE TO POSITVE
PRINT #2, talk$
talk$ = "DCSL 1"    'SET DISCRIMINATOR SLOPE TO NEGATIV
PRINT #2, talk$
talk$ = "BOFF 0"   'SET OFFSET TO 0 s
PRINT #2, talk$
talk$ = "ACMD 0"   'SET TO ACCUMALATE MODE
PRINT #2, talk$

PRINT #2, "DCLV -10E-3"       'SET DISCRIMINATOR"
PRINT #2, "DCLV?"       'QUERY DISCRIMINATOR
INPUT #2, discr!
PRINT "The discriminator is set to:", discr!, "Volts"
 freq = k!
d$ = "FR" + LTRIM$(STR$(freq)) + "MZ"
 PRINT USING "Device = ###, Command = \                    \"; addr%; d$
 CALL absolute(addr%, d$, offset%)
      clk = 1
 WHILE clk <= inttime
      f$ = "d:\AOTFDATA\" + LTRIM$(dat$) + "\" + LTRIM$(dir$) + "\" +
LTRIM$(STR$(clk)) + ".dat"
```

```
    OPEN f$ FOR OUTPUT AS #1    ' FILENAME
    PRINT "The file opened is : ", f$

    PRINT "STARTING SCAN FOR MINUTE #", clk
    PRINT #2, "CLRS"
    scannum = 0
    PRINT #2, "SSCN"
  WHILE scannum < 1200
    PRINT #2, "SCAN?"
    INPUT #2, scannum
  WEND
  PRINT " SCAN COMPLETED FOR MINUTE #", clk
  PRINT " WRITING DATA TO FILE'"
  ct = 0
  WHILE ct < 1024
    talk$ = "BINA?" + LTRIM$(STR$(ct))
    PRINT #2, talk$
    INPUT #2, count$
    PRINT #1, ct, count$
    ct = ct + 1

  WEND
    PRINT "MINUTE COMPLETED"
    clk = clk + 1
    CLOSE #1
  WEND
END
```

```
'THIS PROGRAM IS TO CHECK FOR ALIGNMENT OF FIBER AT PARTICULAR
CONTROL FREQ

' Program to use SRS multichannel scaler/averager SR430
' for measuring  counts with a constant
' discriminator level
' for determining a spectrum of a particular sample using the AOTF
' Configure the SRS430 to 19.2 kbaud, 8 bits, no parity before running the
' program. Use RS232 conection on com1.
'The HP function generator is controlled by the GPIB interface

CLS
PRINT " This program ALIGN.BAS is used to check for alignment of the fiber"
PRINT " at a particular frequency (usually nitrogen line)."
PRINT " The counts at any particular bin can be queried."
PRINT " Once the alignment procedure is done, use LAMP.BAS program to get
the"
PRINT " vertical profile or QSCAN.BAS to step scan."
PRINT
PRINT " This program developed by Anil and Steve on 08/18/97"

'This part of the program controls the HP8656A instrument via GPIB.
'The instrument address is 19. The base address of the card is set to
'&HD000. The I/O address is &H2B8.


DEF SEG = &HD000

'Reset the GPIB card
init% = 0
ioport% = &H2B8
myaddr% = 21
setting% = &H100
PRINT "Reset Card..."
CALL absolute(ioport%, myaddr%, setting%, init%)

'Code to output command string to device
offset% = 3
addr% = 19          ' address of HP8656A instrument

'Turn AM off
d$ = "AMS4"
PRINT USING "Device = ###, Command = \                    \"; addr%; d$
CALL absolute(addr%, d$, offset%)

'Set Amplitude
d$ = "AP1000MV"
PRINT USING "Device = ###, Command = \                    \"; addr%; d$
CALL absolute(addr%, d$, offset%)

'Preset Frequency
d$ = "FR100MZ"
PRINT USING "Device = ###, Command = \                    \"; addr%; d$
CALL absolute(addr%, d$, offset%)
```

```
start:
  PRINT
  PRINT
INPUT "Enter the number of records per scan (1200 records = 1 min): ", rec

INPUT "Enter the frequency (in MHz): ", fstart!

INPUT "Are you sure all the data entered is correct (y/n) :", ans$

IF LCASE$(ans$) = "n" THEN
      GOTO start
ELSE
END IF

' PARAMETERS TO SET BEFORE RUNNING

OPEN "COM1:9600,N,8,2,CS,DS,CD" FOR RANDOM AS #2
talk$ = "OUTP 0"    'DIRECT SR430 OUTPUT TO RS232 PORT
PRINT #2, talk$
talk$ = "BCLK 0"   'SET BINCLOCK TO INTERNAL
PRINT #2, talk$

talk$ = "BWTH 4"   'SET BINWIDTH TO 320 ns
PRINT #2, talk$
talk$ = "BREC 1"    'SET RECORD LENGTH TO 1024 BINS
PRINT #2, talk$

talk$ = "RSCN " + LTRIM$(STR$(rec))    'SET SCANS PER RECORD
PRINT #2, talk$
talk$ = "TRLV 1.0"   'SET TRIGGER LEVEL TO +1.0V
PRINT #2, talk$
talk$ = "TRSL 0"     'SET TRIGGER SLOPE TO POSITVE
PRINT #2, talk$
talk$ = "DCSL 1"     'SET DISCRIMINATOR SLOPE TO NEGATIV
PRINT #2, talk$
talk$ = "BOFF 0"   'SET OFFSET TO 0 s
PRINT #2, talk$
talk$ = "ACMD 0"   'SET TO ACCUMALATE MODE
PRINT #2, talk$

PRINT #2, "DCLV -10E-3"       'SET DISCRIMINATOR"
PRINT #2, "DCLV?"       'QUERY DISCRIMINATOR
INPUT #2, discr!
PRINT "The discriminator is set to:", discr!, "Volts"

  freq = fstart!
 d$ = "FR" + LTRIM$(STR$(freq)) + "MZ"
PRINT USING "Device = ###, Command = \                    \"; addr%; d$
 CALL absolute(addr%, d$, offset%)
      PRINT " Starting counting"
      PRINT #2, "CLRS"
      scannum = 0
      PRINT #2, "SSCN"
```

```
   WHILE scannum < rec
      PRINT #2, "SCAN?"
      INPUT #2, scannum
   WEND
      PRINT " Counting completed"

binchk:

      PRINT
      INPUT " Enter the bin number to be queried (range 0-1023): ", bin
      talk$ = "BINA?" + LTRIM$(STR$(bin))
      PRINT #2, talk$
      INPUT #2, count&
      CLS
      PRINT " The counts at bin", bin, "is:", count&
      PRINT
      INPUT " Do you wish to check another bin [y/n]: ", ans$
      IF LCASE$(ans$) = "y" THEN
      GOTO binchk
      ELSE
      END IF
      PRINT
      INPUT " Do you wish to do another scan [y/n]: ", ans2$
      IF LCASE$(ans2$) = "y" THEN
      CLOSE #2
      GOTO start
      ELSE
      END IF
      PRINT
      PRINT " Thanks for using this nifty program "
END
```

'THIS PROGRAM IS STEP SCANNING A FREQUENCY RANGE

```
' Program to use SRS multichannel scaler/averager SR430
' for measuring  counts with a constant
' discriminator level
' for determining a spectrum of a particular sample using the AOTF
' Configure the SRS430 to 19.2 kbaud, 8 bits, no parity before running the
' program. Use RS232 conection on com1.
'The HP function generator is controlled by the GPIB interface

CLS
PRINT " This program QSCAN.BAS is used to scan over a frequency range and"
PRINT " look for a particular species without a range resolution. "
PRINT " Once the frequency is determined, use LAMP.BAS program to get the"
PRINT " vertical profile."
PRINT " For alignment, use ALIGN.BAS program"
PRINT
PRINT " This program developed by Anil and Steve on 08/18/97"

'This part of the program controls the HP8656A instrument via GPIB.
'The instrument address is 19. The base address of the card is set to
'&HD000. The I/O address is &H2B8.


DEF SEG = &HD000

'Reset the GPIB card
init% = 0
ioport% = &H2B8
myaddr% = 21
setting% = &H100
PRINT "Reset Card..."
CALL absolute(ioport%, myaddr%, setting%, init%)

'Code to output command string to device
offset% = 3
addr% = 19          ' address of HP8656A instrument

'Turn AM off
d$ = "AMS4"
PRINT USING "Device = ###, Command = \                    \"; addr%; d$
CALL absolute(addr%, d$, offset%)

'Set Amplitude
d$ = "AP1000MV"
PRINT USING "Device = ###, Command = \                    \"; addr%; d$
CALL absolute(addr%, d$, offset%)

'Preset Frequency
d$ = "FR100MZ"
PRINT USING "Device = ###, Command = \                    \"; addr%; d$
CALL absolute(addr%, d$, offset%)

start:
  PRINT
```

```
  PRINT

  INPUT "Enter today's date: ", dat$
INPUT "Enter the number of records per scan (1200 records = 1 min): ", rec
INPUT "Enter the number of bins to accumalate ( 1 bin = 320 ns(100 m): ", tbin
INPUT "Enter the name of the file to store the data: ", file$
t$ = "d:\STEPSCAN\" + LTRIM$(dat$)

g$ = "d:\TOM\param.dat"
OPEN g$ FOR OUTPUT AS #5

INPUT "Enter the starting frequency (in MHz): ", fstart!
INPUT "Enter the ending frequency (in MHz): ", fend!
INPUT "Enter the frequency increment (in MHz): ", fincr!

INPUT "Are you sure all the data entered is correct (y/n) :", ans$

IF LCASE$(ans$) = "n" THEN
      GOTO start

ELSE
END IF


ON ERROR GOTO newdir
MKDIR t$
newdir:

f$ = "d:\STEPSCAN\" + LTRIM$(dat$) + "\" + LTRIM$(file$)
OPEN f$ FOR OUTPUT AS #1    ' FILENAME
PRINT "The file opened is : ", f$

'OPEN g$ FOR OUTPUT AS #5
WRITE #5, file$, fstart!, fend!, incr!
CLOSE #5
' PARAMETERS TO SET BEFORE RUNNING

OPEN "COM1:9600,N,8,2,CS,DS,CD" FOR RANDOM AS #2
talk$ = "OUTP 0"    'DIRECT SR430 OUTPUT TO RS232 PORT
PRINT #2, talk$
talk$ = "BCLK 0"   'SET BINCLOCK TO INTERNAL
PRINT #2, talk$

talk$ = "BWTH 4"   'SET BINWIDTH TO 320 ns
PRINT #2, talk$
talk$ = "BREC 1"    'SET RECORD LENGTH TO 1024 BINS
PRINT #2, talk$

talk$ = "RSCN " + LTRIM$(STR$(rec))    'SET SCANS PER RECORD
PRINT #2, talk$
talk$ = "TRLV 1.0"   'SET TRIGGER LEVEL TO +1.0V
PRINT #2, talk$
talk$ = "TRSL 0"     'SET TRIGGER SLOPE TO POSITVE
PRINT #2, talk$
```

```
talk$ = "DCSL 1"     'SET DISCRIMINATOR SLOPE TO NEGATIV
PRINT #2, talk$
talk$ = "BOFF 0"   'SET OFFSET TO 0 s
PRINT #2, talk$
talk$ = "ACMD 0"   'SET TO ACCUMALATE MODE
PRINT #2, talk$

PRINT #2, "DCLV -10E-3"       'SET DISCRIMINATOR"
PRINT #2, "DCLV?"       'QUERY DISCRIMINATOR
INPUT #2, discr!
PRINT "The discriminator is set to:", discr!, "Volts"
  k! = fstart!
  WHILE k! <= fend!
  PRINT #2, "CLRS"
     scannum = 0
     PRINT #2, "SSCN"
  WHILE scannum < rec
     PRINT #2, "SCAN?"
     INPUT #2, scannum
  WEND
  bin = 0
  tcount& = 0
  WHILE bin < tbin
     talk$ = "BINA?" + LTRIM$(STR$(bin))
     PRINT #2, talk$
     INPUT #2, count&
     tcount& = tcount& + count&
     bin = bin + 1
  WEND
     PRINT #1, k!, tcount&
     PRINT k!, tcount&
     k! = k! + fincr!
  WEND

  CLOSE #1
  PRINT " COMPLETED WITHOUT ERRORS (hopefully)"
  END
```